Published online 12 October 2020

Nucleic Acids Research, 2020, Vol. 48, No. 19 ***10785–10801***
doi: 10.1093/nar/gkaa797

Reversible regulation of conjugation of *Bacillus subtilis* plasmid pLS20 by the quorum sensing peptide responsive anti-repressor Rap_{pLS20}

Praveen K. Singh[1], Ester Serrano[1], Gayetri Ramachandran[1], Andrés Miguel-Arribas[1], César Gago-Cordoba[1], Jorge Val-Calvo[1], Arancha López-Pérez[1], Carlos Alfonso[2], Ling Juan Wu[3], Juan R. Luque-Ortega[4,*] and Wilfried J.J. Meijer[1,*]

[1]Centro de Biología Molecular "Severo Ochoa" (CSIC-UAM), C. Nicolás Cabrera 1, Universidad Autónoma, Canto Blanco, 28049 Madrid, Spain, [2]Centro de Investigaciones Biológicas Margarita Salas (CSIC), C. Ramiro de Maeztu 9, 28040 Madrid, Spain, [3]Centre for Bacterial Cell Biology, Biosciences Institute, Newcastle University, Newcastle upon Tyne, UK and [4]Molecular Interactions Facility, Centro de Investigaciones Biológicas Margarita Salas (CSIC), C. Ramiro de Maeztu 9, 28040 Madrid, Spain

Received July 29, 2020; Revised September 02, 2020; Editorial Decision September 09, 2020; Accepted September 14, 2020

ABSTRACT

Quorum sensing plays crucial roles in bacterial communication including in the process of conjugation, which has large economical and health-related impacts by spreading antibiotic resistance. The conjugative *Bacillus subtilis* plasmid pLS20 uses quorum sensing to determine when to activate the conjugation genes. The main conjugation promoter, P_c, is by default repressed by a regulator Rco_{pLS20} involving DNA looping. A plasmid-encoded signalling peptide, Phr^*_{pLS20}, inactivates the anti-repressor of Rco_{pLS20}, named Rap_{pLS20}, which belongs to the large group of RRNPP family of regulatory proteins. Here we show that DNA looping occurs through interactions between two Rco_{pLS20} tetramers, each bound to an operator site. We determined the relative promoter strengths for all the promoters involved in synthesizing the regulatory proteins of the conjugation genes, and constructed an *in vivo* system uncoupling these regulatory genes to show that Rap_{pLS20} is sufficient for activating conjugation *in vivo*. We also show that Rap_{pLS20} actively detaches Rco_{pLS20} from DNA by preferentially acting on the Rco_{pLS20} molecules involved in DNA looping, resulting in sequestration but not inactivation of Rco_{pLS20}. Finally, results presented here in combination with our previous results show that activation of conjugation inhibits competence and competence development inhibits conjugation, indicating that both processes are mutually exclusive.

GRAPHICAL ABSTRACT

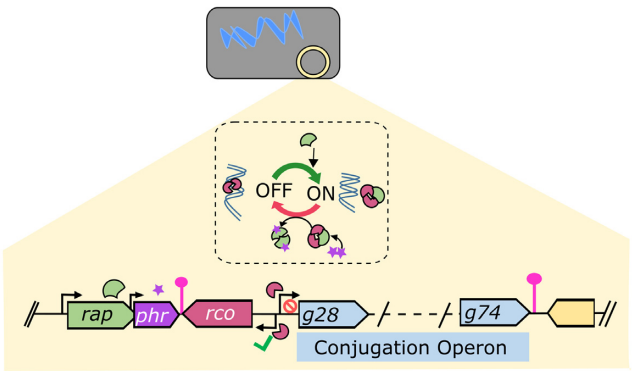

INTRODUCTION

Bacterial communication, through a process named quorum sensing by secreting and sensing signalling peptides (1,2), allows bacterial communities to adapt and coordinate

*To whom correspondence should be addressed. Tel: +34 91 196 4539; Fax: +34 91 196 4420; Email: wmeijer@cbm.csic.es
Correspondence may also be addressed to Juan R. Luque-Ortega. Tel: +34 91 837 3112 (Ext 4297); Fax: +34 91 536 04 32; Email: luque@cib.csic.es
Present addresses:
Praveen K. Singh, Max Planck Institute for Terrestrial Microbiology, Karl-von-Frisch-Straße 10, Marburg 35043, Germany.
Gayetri Ramachandran, Laboratory of Host-Microbiota Interaction, Institut Necker Enfants Malades (INEM)-INSERM 1151, Université Paris Descartes-Sorbonne Paris Cité, 156–160, rue de Vaugirard, 75015 Paris, France.
Ester Serrano, Institute of Infection, Immunity and Inflammation, University of Glasgow, Glasgow G12 8TA, UK.
Arancha López-Pérez, AiCuris Anti-infective Cures GmbH, Friedrich-Ebert-Str.475 / Geb.302, 42117 Wuppertal, Germany.

their survival strategy when encountering adverse conditions by changing their expression profile. In Gram-positive (G+) bacteria, the signalling molecules, aka pheromones, are small extracellular peptides often ranging between 5 and 10 residues. They can interact with sensor kinases embedded in the bacterial membrane that form part of the two-component systems, or be (re)imported inside the cell where they then interact with cytosolic receptor molecules (3–6). A large number of cytoplasmic signal-peptide receptor proteins belong to the so-called RRNPP family of proteins, named after its prototypical members Rap, Rgg, NprR, PlcR and PrgX (for review see, 7,8–10). Most of the genes encoding the RRNPP proteins in the phylum of Firmicutes are co-transcribed with the gene encoding the signalling peptide. The signalling peptides are synthesized as a pre-propeptide, which is cleaved again after being secreted to become the mature peptide. The mature peptide generally corresponds to the C-terminal region of the pre-proprotein, and can be imported inside the cell by the oligopeptide permease system (3,6). The RRNPP proteins are characterized by a two-domain structure that is composed of a large signal peptide binding C-terminal domain containing multiple tetratricopeptide repeats (TPR), and a smaller three α-helical N-terminal effector domain. Binding of the signalling peptide to the C-terminal TPR domain modulates interaction or activity of the effector domain with its ligand resulting in downstream regulatory effects. The effector domains can be classified into three groups: many adopt a helix-turn-helix (HTH) conformation allowing them to bind DNA thereby repressing gene expression; some interact with a target protein, for example a transcriptional regulator, and modulate gene expression directly or indirectly; and some have phosphatase activity, which allow them to interfere with phosphorylation relay involved in phosphorylation-mediated activation of Spo0A, the master regulator of sporulation in *Bacillus subtilis*.

RRNPP-mediated quorum sensing mechanisms are involved in various cellular processes such as regulation of differentiation pathways like sporulation and competence, activation of virulence genes and altering surface characteristics (9–11). Interestingly, some RRNPP proteins play crucial roles in horizontal gene transfer events, for example, by determining whether a phage enters the lytic or lysogenic cycle (12), or by regulating the expression of conjugation genes present on a conjugative element. Conjugation is the process by which a conjugative DNA element is transferred from a donor to a recipient cell through a sophisticated pore that connects both cells. Conjugative elements can be present on a plasmid, which are then named conjugative plasmids, or they can be embedded within a bacterial genome and are then named integrative and conjugative element (ICE) (13, for review see 14). Conjugation is the main horizontal gene transfer route that is responsible for the spread of antibiotic resistance and virulence genes and therefore poses a serious worldwide problem (15–18). In addition to genes carried on the plasmid, conjugative plasmids can also mobilize the transfer of co-resident rolling-circle type plasmids, many of which contain antibiotic/virulence genes (19). For example, the *B. subtilis* conjugative plasmid pLS20 itself encodes a putative VanZ protein that would confer resistance to the antibiotic teicoplanin (our unpublished results, 20). In addition, it can disseminate antibiotic-resistance genes carried by several rolling circle plasmids like pUB110, pBC16, pMV158 and pTB913 by mobilizing them (21–23). Examples of RRNPP proteins that regulate the transfer of conjugative elements are RapI of the *B. subtilis* ICE element ICE*Bs*1, PrgX of the *Enterococcus faecalis* plasmid pCF10, which harbours a tetracycline resistance gene (24), and Rap_{pLS20} of the *B. subtilis* plasmid pLS20 (25–27).

Curiously, the RRNPP proteins RapI, PrgX and Rap_{pLS20} regulate expression of the conjugation genes in very different ways. Plasmid pCF10-encoded PrgX is a DNA-binding protein that can interact with two signal peptides exerting opposing effects on DNA binding. Interaction of the plasmid encoded iCF10 with PrgX favours a conformation in which PrgX binds to DNA resulting in repression of the conjugation genes, while binding of the recipient cell encoded cCF10 alters the conformation of PrgX and relieves PrgX-mediated repression (8). In the case of ICE*Bs*1, the conjugation genes are repressed by a repressor named ImmR. Inactivation of ImmR, which results in activation of the conjugation genes and hence conjugative transfer of the ICE, can occur in two ways. First, as a consequence of RecA-dependent SOS response to DNA damage, or second, when RapI stimulates the ICE-encoded protease ImmA to degrade ImmR (28).

The conjugation genes of plasmid pLS20, repressed by a plasmid encoded transcriptional regulator named Rco_{pLS20}, is relieved by Rap_{pLS20} (27). As for RapI of ICE*Bs1*, Rap_{pLS20} activates conjugation in the absence or presence of low concentrations of its cognate mature signalling peptide Phr^*_{pLS20}, and at higher levels Phr^*_{pLS20} inactivates Rap_{pLS20}. Phr^*_{pLS20} concentrations will be relatively high or low when donor cells are predominantly surrounded by donor or recipient cells, respectively. Hence, conjugation will become activated only under conditions in which recipient cells are potentially present. The pLS20 conjugation genes are located in a single large operon that is under the control of the strong conjugation promoter P_c. At its left side, the conjugation operon is flanked by the divergently oriented regulatory gene rco_{pLS20} and the weak P_r promoter controlling rco_{pLS20} expression that overlaps with the P_c promoter. The intergenic region encompassing the P_c and P_r promoters contains two Rco_{pLS20} operators, O_I and O_{II}, separated by 75 bp. Binding of Rco_{pLS20} to both operators results in DNA looping and causes tight repression of the conjugation promoter P_c. Simultaneously, Rco_{pLS20} regulates its own expression: at low and high Rco_{pLS20} concentrations the P_r promoter is activated and repressed, respectively. Phr^*_{pLS20}-unbound Rap_{pLS20} activates conjugation by relieving Rco_{pLS20}-mediated P_c repression, and binding of the peptide antagonizes the antirepressive function of Rap_{pLS20}, reverting the system to its default state (13,27). This multi-layered DNA-looped genetic switch tightly blocks expression of the conjugation genes under conditions unfavourable for conjugation while being sensitive to activate accurately the conjugation genes when appropriate conditions occur.

Here, we have studied various unaddressed aspects of this regulatory circuit. We demonstrate that phr_{pLS20} expression is controlled by two promoters, and we have determined

the relative strengths of promoter P_c and the promoters of the genes regulating its activity. We found that the multi-layered regulation of P_c results in population scale on/off switching. We show that Rap_{pLS20} is sufficient to relieve Rco_{pLS20}-mediated repression of the P_c promoter *in vivo*, by interacting directly with Rco_{pLS20}. We also show that each Rco_{pLS20} operator is bound by one Rco_{pLS20} tetramer and that DNA looping is achieved through interactions between the two operator-bound Rco_{pLS20} tetramers, contrary to what has been proposed before. Interestingly, Rap_{pLS20} preferentially acts to interrupt DNA looping. Finally, Phr^*_{pLS20} shares high similarity to the host-encoded PhrF, and PhrF and derivatives can bind and inactivate Rap_{pLS20}, suggesting that pLS20 conjugation may be influenced by the host RapF/PhrF signalling pathway.

MATERIALS AND METHODS

Bacterial strains, plasmids and media

Bacterial cultures were grown in LB broth or on LB agar at 37°C except BTH101, which was grown at 30°C. Where appropriate the following antibiotics were added to the media: ampicillin (100 μg/ml), erythromycin (1 and 150 μg/ml for *B. subtilis* and *Escherichia coli*, respectively, chloramphenicol (5 μg/ml), spectinomycin (100 μg/ml), and kanamycin (10 μg/ml). *E. coli* BTH101 was used as the reporter strain for the BACTH system. For BACTH assay, minimal medium M63 supplemented with maltose was used for growth (29,30). Strains and plasmids used are listed in Supplemental Table S1. All *B. subtilis* strains are isogenic to *B. subtilis* strain 168 (Bacillus Genetic Stock Centre Code 1A700). Oligonucleotides used (Isogen Life Sciences, The Netherlands) are listed in Supplemental Table S2. See supplemental material for construction of plasmids and strains. Phr^*_{pLS20}, PhrF*, PhrF*-R2K and PhrF*-I5Y peptides were synthesized by the Protein Chemistry facility of the CIB Institute.

Transformation

Escherichia coli cells were transformed using standard methods as previously described (31). For standard *B. subtilis* transformations, competent cells were prepared as described by Bron (32). For making knockout version of pLS20cat, high competency protocol was used as described by Zhang and Zhang (33). For co-transformation of plasmids for BACTH assay, electro-competent cells of *E. coli* were prepared as described earlier (31).

Conjugation assays

Unless specified otherwise, conjugation was carried out in liquid medium as described earlier (27). Thus, for standard conjugation experiments, overnight cultures of donor and recipient cells, grown in the presence of appropriate antibiotics, were diluted 50-fold in fresh 37°C pre-warmed LB medium without antibiotics and grown in shaking (180 rpm) water bath until an OD_{600} between 0.9 and 1 was reached. Next, 200 μl of both donor and recipient cells were mixed in 2.5 ml eppendorf tube and incubated for 15 min at 37°C without shaking to permit conjugation. Finally, appropriate dilutions were plated on LB agar plates supplemented with proper antibiotics to select either for transconjugants or for donor cells. When conjugation efficiencies were determined as a function of growth, overnight cultures were diluted to an OD_{600} of 0.01. Next, donor and recipient cells were grown separately (180 rpm) and 200 μl of the donor and recipient cultures were withdrawn at different times and proceeded as described above. Growth was followed by measuring OD_{600} at regular intervals. In order to study the effect on conjugation of over-expression of a given gene placed under the control of the inducible P_{spank} promoter, IPTG was added to prewarmed LB medium used for inoculation of the overnight grown cultures. Unless mentioned otherwise, IPTG was added to a final concentration of 1 mM. All conjugation experiments were repeated at least three times. The entry into stationary growth ($t = 0$) is determined in retrospect based on the growth curve. Consequently, time points at which samples were taken fluctuate slightly between each experiment. Values for specific time points extrapolated from the curves of repeated experiments showed that they differed by <10%.

Flow cytometry

Overnight grown cultures were diluted 100-fold in prewarmed LB medium. Two milliliters of the culture were centrifuged (1 min 14 000 *g*) when the OD_{600} was between 0.8 and 1.0. After a washing step (2 ml 0.2 μM filtered 1× PBS), the pellet was resuspended in 1 ml 0.2 μM filtered 1× PBS. Next, cells were directly measured on a FacsCalibur cytometer (Becton Dickinson, United States) equipped with an argon laser (488 nm). The fluorescence of at least 100 000 cells was analysed using a 530/30 nm band pass filter using arbitrary units (AU). Sample data were collected using CellQuest Pro (Becton Dickinson, United States) software and analysed afterwards using FlowJo 6.4.1 mac (TreeStar, United States) software. *B. subtilis* strain 168 was included in each flow cytometry experiment as negative control. Values showed and represented in graphs, corresponds with Geomean estimated by FlowJo.

Fluorescence microscopy

Cells grown in LB medium with/out chloramphenicol or spectinomycin were placed on agarose pads as described previously (27). Images were acquired using a Nikon Eclipse Ti-U inverted epifluorescence microscope and a QImaging Rolera EM-C2 EM-CCD Camera under 100× phase oil objective, and were processed using MetaMorph software. TIFF images were further processed in Inkscape.

Rap_{pLS20}-$His_{(6)}$ purification

An overnight culture of *E. coli* BL21 (DE3) carrying plasmid pEST10_B was used to inoculate (100-fold dilution) 1 L of fresh LB medium containing 30 μg/ml of kanamycin and incubated at 37°C with shaking. At OD_{600} of 0.5, rap_{pLS20}-$His_{(6)}$ was induced with 1 mM IPTG at 37°C and growth was continued for 2 h. Cells were collected by centrifugation and washed in 1/10 vol. of buffer A (250 mM NaCl, 10

mM $MgCl_2$, 20 mM Tris–HCl pH 8, 7% glycerol, 10 mM imidazole, 1 mM β-mercaptoethanol). Next, cells were centrifuged and re-suspended in 1/3 volume of buffer A and they were lysed by sonication followed by DNase I treatment for 30 min at 4°C. Next, the lysate was centrifuged twice (15k, 30 min) and the supernatant was collected and mixed with 1 ml of nickel NTA agarose beads equilibrated with buffer A. The mixture was incubated end-over-end for 1 h at 4°C then packed into a column. The column was washed with extensive amounts (> 50 column volumes) of buffer A containing increasing concentrations (10, 20, 30, 50 and 100 mM) of imidazole. Next, the Rap_{pLS20}-$His_{(6)}$ protein was eluted in eight fractions of 1 ml of buffer A containing 500 mM imidazole. All fractions were analysed by SDS-PAGE and only the fractions with >95% purity were pooled, dialyzed against buffer B (20 mM Tris–HCl pH 8.0,1 mM EDTA, 250 mM NaCl, 10 mM $MgCl_2$, 7mM β-mercaptoethanol, 20% v/v glycerol) and stored in aliquots at –80°C. Protein concentrations were determined by Bradford assay.

EMSA and Southern blotting

The gel retardation assays were carried out as described earlier (34). Thus, different fragments of intergenic regions between gene *28* and *rco_{pLS20}* were amplified by PCR using pLS20cat as template. The resulting PCR fragments were purified and equal concentrations (300 nM) were incubated on ice in binding buffer [20 mM Tris HCl pH 8, 1 mM EDTA, 5 mM $MgCl_2$, 0.5 mM DTT, 100 mM KCl, 10% (v/v) glycerol, 0.05 mg ml^{-1} BSA] without and with increasing amounts of purified Rco_{pLS20}-$His_{(6)}$ or Rap_{pLS20}-$His_{(6)}$ in a total volume of 16 μl. After careful mixing, samples were incubated for 20 min at 30°C, placed back on ice for 10 min, and then loaded onto 2% agarose gel in 0.5XTBE. Electrophoresis was carried out in 0.5XTBE at 50 V at 4°C. Finally, the gel was stained with ethidium bromide, de-stained in 0.5× TBE and photographed with UV illumination.

The fragments F-A and F-B applied in EMSA and subsequent Southern blot experiments were generated by PCR using as template plasmids pGR49A and primer sets [oGR154-oGR155] and [oGR153-oGR161], respectively. The probes specific for Fragment F-A and F-B were also generated by PCR and pGR49A as template in combination with primer sets [oGR155-oGR163] and [oGR156-oGR162], respectively. The DNA probes were labelled with horseradish peroxidase (HRP) enzyme using glutaraldehyde provided by the ECL Direct Nucleic Acid Labelling and Detection kit (Amersham Biosciences). The conditions for EMSA were equal to those described above. After electrophoresis the gel was first submerged in a depurination solution (250 mM HCl solution) until the bromophenol blue dye had turned completely yellow (10 min), then in a solution of 1 M NaCl and 0.5 M NaOH to denature the DNA until the bromophenol dye regained its blue colour (30 min), and finally for 30 min in a solution of 1.5 M NaCl and 0.5 Tris–HCl at pH 7.5 to neutralize the gel. Next, the DNA was transferred to a positively charged nylon membrane (Amersham Hybrid N^+ Membrane) using capillary blotting (31). After transfer, the DNA was fixed to the nylon membrane by UV crosslinking using a Stratagene UV Crosslinker. For detection, the membrane was prehybridized for 1 h in hybridization buffer [5× SSC, 2% (w/v) blocking reagent, 0·1% (w/v) *N*-laurosylsarcosine, 7% (w/v) SDS, 50 mM sodium phosphate buffer (pH 7.0), 50% (v/v) formamide] at 42 °C. Hybridization was carried out at 42°C overnight in hybridization buffer containing the denatured probe. After hybridization, the membrane was washed twice in primary wash buffer (0.5× SSC, 6 M urea and 0.4% SDS) at 42°C for 20 min each, and then washed twice in secondary wash buffer (2× SSC) at room temperature for 5 min each. Hybridized probes were detected following the manufacturer's guidelines.

BACTH experiments

The bacterial adenylate cyclase-based two-hybrid (BACTH) system assay (Agilent technologies) was used to identify homogenous and heterogeneous interactions between Rco_{pLS20} and Rap_{pLS20}. To perform these experiments, the genes encoding Rco_{pLS20} and Rap_{pLS20} proteins were cloned in frame with DNA regions encoding the C- and N-terminal of T18- and T25-domain of Cya protein from *Bordetella pertussis* in all possible combinations as explained in Supplemental Figure S7. T18 and T25 fragments were present on two different plasmids pUT18 and pKT25, which contain different antibiotic resistance markers (ampicillin and kanamycin, respectively). Different combinations of final plasmids were co-transformed in BTH101 competent cells to have all kinds of interactions between and within Rco_{pLS20} and Rap_{pLS20}.

Sedimentation velocity assays (SV)

Protein and DNA samples in buffer 20 mM Tris, 250 mM NaCl, 10 mM $MgCl_2$, 1 mM EDTA, 0.1 mM β-mercaptoethanol and 1% glycerol, pH 7.4, were loaded (320 μL) into 12 mm Epon-charcoal standard double-sector centerpieces and centrifuged in a XL-I analytical ultracentrifuge (Beckman-Coulter Inc.) equipped with both UV-VIS absorbance and Raleigh interference detection systems, using an An-50Ti rotor. SV assays were performed at 48 000 rpm (167 700 *g*) in the case of proteins, and at 43 000 rpm (134 600 *g*) for DNA and protein–DNA complexes, and sedimentation profiles were recorded by absorbance at 280, 260 or 230 nm. Differential sedimentation coefficient distributions were calculated by least-squares boundary modelling of sedimentation velocity data using the continuous distribution c(*s*) Lamm equation model as implemented by SEDFIT (35). These experimental s values were corrected to standard conditions using the program SEDNTERP (36) to get the corresponding standard s values ($s_{20,w}$). Protein-protein and protein–DNA interactions were analysed by multi-signal sedimentation velocity (MSSV). Data were globally analysed by SEDPHAT software (37) using the 'multiwavelength discrete/continuous distribution analysis' model, to determine the spectral and diffusion-deconvoluted sedimentation coefficient distributions, $c_k(s)$, from which the number and stoichiometry of Rap_{pLS20} versus Rco_{pLS20} or Rco_{pLS20} versus DNA molecules can be derived (38). Prediction of extinction coefficients for DNA

fragment III considering duplex hypochromism at 260 nm was done by means of the Microsoft Excel® application developed by Tataurov (39).

Sedimentation equilibrium assays (SE)

Short columns (95 μl) SE experiments of Rap_{pLS20} were carried out at speeds ranging from 7000 to 10 000 rpm (3900–7900 *g*) and data collected at 280 nm, using the same experimental conditions and instrument as in the SV experiments. A last high-speed run at 48 000 rpm (167 700 *g*) was done to deplete protein from the meniscus region to obtain the corresponding baseline offsets. Weight-average buoyant molecular weights of Rap_{pLS20}, alone or in the presence of the pentapeptides, were obtained by fitting a single-species model to the experimental data using the HeteroAnalysis program (40), once corrected for temperature and solvent composition with the program SEDNTERP (36). Equilibrium binding isotherms of Rap_{pLS20} with different pentapeptides were built using a fixed Rap_{pLS20} concentration of 6 μM titrated with increasing concentrations of each pentapeptide (from 0.3 to 30 μM). The oligomerization state of Rap_{pLS20} was determined from the experimental apparent buoyant mass increments, using 0.7363 as partial specific volume, calculated from its amino acid composition by SEDNTERP. The data were modelled with a three parameter Hill function, as implemented in SigmaPlot 11.0 software.

Computer-assisted analysis

ClustalW was used to align *B. subtilis* and pLS20-encoded Phr proteins. All graphics work was done by using inkscape (https://inkscape.org/). NIS Elements AR Analysis software provided by Nikon Instruments were used to analyse time lapse video of conjugating cells (https://www.microscope.healthcare.nikon.com/products/software/nis-elements/nis-elements-advanced-research). Graphics were plotted using Excel or Sigmaplot programs.

RESULTS

Rap_{pLS20} alone is sufficient to relief Rco_{pLS20}-mediated repression of the P_c promoter *in vivo*

We have previously shown that the transcriptional regulator Rco_{pLS20} represses the main pLS20 conjugation promoter P_c, and that Rap_{pLS20} activates conjugation by relieving Rco_{pLS20}-mediated repression of the conjugation genes (27,34). However, it was not clear if pLS20-encoded protein(s) other than Rap_{pLS20} are required to activate the P_c promoter, or how Rap_{pLS20} relieves Rco_{pLS20}-mediated repression of the P_c promoter. As a first approach to address these questions, we constructed an *in vivo B. subtilis* system in which the rco_{pLS20} and rap_{pLS20} genes are uncoupled from their native setting and were placed under different inducible promoters, combined with a P_c-*lacZ* reporter gene. Thus, we constructed strain PKS25 (*amyE*::P_{spank}-rco_{pLS20}, *lacA*::P_{xyl}-rap_{pLS20}, *thrC*::P_c-*lacZ*; [P_{spank} and P_{xyl} are an IPTG- and xylose-inducible promoter, respectively]). PKS25 cells were plated on Xgal-containing LB agar plates with or without addition of one or both inducers, and the colour of the overnight grown colonies was used as an indicator of the P_c promoter activity. An overview of the results is presented in Figure 1, representative images of colony colours are shown in Supplemental Figure S1. In the absence of either inducer the P_c promoter was active and hence colonies turn blue, but colonies were white in the presence of only IPTG, which is in agreement with our previous results (34) showing that induction of rco_{pLS20} resulted in repression of the P_c promoter. Colonies regained the blue colour when both rco_{pLS20} and rap_{pLS20} were expressed (plates containing both IPTG and xylose). This shows that Rap_{pLS20} alone is sufficient to relieve Rco_{pLS20}-mediated repression of the P_c promoter. A control experiment showed that expression of Rap_{pLS20} alone did not affect activity of the P_c promoter (see Supplemental Figure S2).

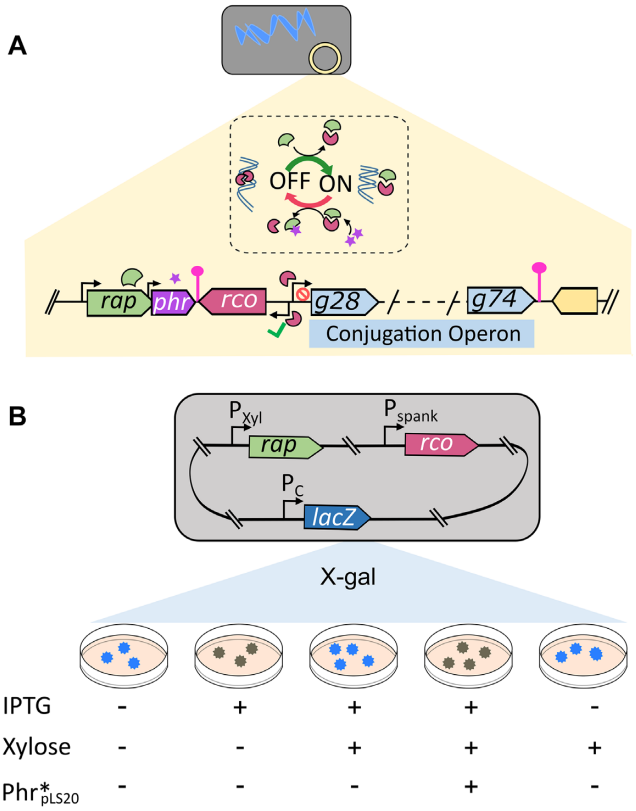

Figure 1. Evidence that the circuit regulating activity of the main conjugation promoter P_c is composed of Rco_{pLS20}, Rap_{pLS20} and Phr^*_{pLS20}. (**A**) Schematic genetic map of the conjugation operon and upstream genes rap_{pLS20} (green arrow, *rap*), phr_{pLS20} (purple arrow, *phr*) and rco_{pLS20} (red arrow, *rco*). Rco_{pLS20} is a transcriptional regulator: it represses the P_c promoter and activates its own promotor P_r. Rap_{pLS20} is an antirepressor of Rco_{pLS20}. The Phr^*_{pLS20} signalling peptide inactivates Rap_{pLS20}. See text for further details. Position and direction of promoters are indicated with bent arrows. Transcriptional terminators are indicated with violet lollipop symbols. Proteins Rap_{pLS20} and Rco_{pLS20} are indicated above their corresponding genes using the same colour code. Mature Phr^*_{pLS20} pentapeptide is indicated by purple stars. (**B**) Regulation of the P_c promoter in an uncoupled *in vivo* system. PKS25 cells (*amyE*::P_{spank}-rco_{pLS20}, *lacA*::P_{xyl}-rap_{pLS20}, *thrC*::P_c-*lacZ*) were plated on Xgal-containing plates that were supplemented or not with IPTG (10 μM), xylose (1%), synthetic Phr^*_{pLS20} peptide (10 μM), and screened after overnight incubation at 37°C.

The activity of other known Rap proteins is regulated by a five or six-residue peptide encoded by a small *phr*

gene mostly located directly downstream of the *rap* genes, and whose primary product is subject to a secretion-processing-import pathway (3). A *phr* gene, phr_{pLS20}, is located downstream of rap_{pLS20} and addition of the mature 5-residue peptide Phr^*_{pLS20} to cultures inhibited conjugation (27). Whereas this indicated that Phr^*_{pLS20} inactivates Rap_{pLS20}, it did not exclude the possibility that inactivation of Rap_{pLS20} required, besides Phr^*_{pLS20}, other pLS20-encoded protein(s). To address this issue, we plated PKS25 cells onto plates containing, besides X-gal, IPTG and xylose, also mature Phr^*_{pLS20} peptide. As shown in Figure 1 and Supplemental Figure S1, colonies grown on these plates were white, demonstrating that Phr^*_{pLS20} is required and sufficient to inactivate Rap_{pLS20}.

The *B. subtilis* encoded PhrF* signalling peptide interacts with Rap_{pLS20} *in vitro* and is able to inactivate Rap_{pLS20} *in vivo*

The *B. subtilis* genome encodes 11 *rap* genes, eight of which are directly followed by a Phr* encoding gene (3,41). When the full-length pre-protein Phr sequence encoded by pLS20 was aligned with those encoded by the *B. subtilis* genome (Figure 2A), it was clear that the sequence of the mature PhrF* pentapeptide is very similar to that of Phr^*_{pLS20}: residues at positions 1, 3 and 4 are identical; position 2 concerns a conserved substitution of Lysine to Arginine, and position 5 a change from Tyrosine to Isoleucine. The high level of similarity between PhrF* and Phr^*_{pLS20} was surprising and we wondered whether there might be cross talk between PhrF* and Rap_{pLS20}, and if so, whether PhrF* might affect pLS20 conjugation. Besides PhrF*, we also tested two synthetic variants, PhrF*-I5Y, and PhrF*-R2K, that can be considered intermediates between PhrF* and Phr^*_{pLS20} because they contain only one difference (see Figure 2B). Recently, we have shown that binding of Phr^*_{pLS20} inactivates Rap_{pLS20} by altering its oligomerization state from dimer to tetramer (42). We therefore used sedimentation velocity (SV) analytical ultracentrifugation (AUC) experiments to test if PhrF* and its two variants PhrF*-I5Y and PhrF*-R2K could inactivate Rap_{pLS20} as does Phr^*_{pLS20}, by determining the oligomerization state of Rap_{pLS20} in the presence of these peptides. As shown in Figure 2C, when added in a 10-fold excess all the peptides tested caused tetramerization of Rap_{pLS20}, indicating that they all could interact with Rap_{pLS20}. To determine the possible effects of the amino acid differences between PhrF* and Phr^*_{pLS20} on the affinity of these peptides for Rap_{pLS20}, we performed a series of sedimentation equilibrium (SE) assays. In these experiments, the pentapeptide variants PhrF*-I5Y and PhrF*-R2K were also included to determine the possible differential effects of either of the two residues. A fixed Rap_{pLS20} concentration of 6 μM was titrated with increasing peptide concentrations (from 0.3 to 30 μM). Figure 2D shows the binding isotherms built from the experimental buoyant mass increments obtained at low speed and 280 nm, through an empirical three parameters Hill plot (equation 1):

$$y = \frac{a x^b}{K_d{}^b + x^b}$$

where y stands for the increase in the buoyant mass, a denotes the maximum buoyant mass increase at saturation, x is the total concentration of peptide, K_d is the peptide concentration at half-maximal buoyant mass increase and b is an empirical cooperativity parameter. Taking into account that the maximal buoyant mass increase obtained at the highest peptide concentration corresponds to the Rap_{pLS20} tetramer, as experimentally determined by the previous SE assays, a tetramerization model can explain the experimental binding isotherm obtained with Phr^*_{pLS20}, with a macroscopic K_d of 2.1 ± 0.1 μM. Analogously, for PhrF*, a tetramerization model can account for the binding isotherm with a macroscopic K_d of 5.3 ± 0.1 μM, evidencing the down-modulating effect of the two substitutions within its amino acid sequence. Both PhrF*-I5Y and PhrF*-R2K, induced Rap_{pLS20} tetramerization with a macroscopic K_d of 4.2 ± 0.1 μM as shown in Figure 2D, indicating that the residues at positions 2 and 5 of Phr^*_{pLS20} were both important and that they contributed similarly to the specificity of the peptide Rap_{pLS20} interaction.

Next, we tested if the native PhrF* and its variants PhrF*-R2K and PhrF*-I5Y had an effect *in vivo*. For this we plated PKS25 cells onto LB agar plates containing Xgal and 10 μM IPTG, and supplemented with different concentration of Phr^*_{pLS20}, PhrF*, PhrF*-R2K or PhrF*-I5Y. The results obtained are shown in Supplementary Figure S3 and a summary is given in Figure 2E. As expected, colonies were blue in the absence or presence of very low amounts of $PhrF^*_{pLS20}$, indicating that Rap_{pLS20} relieved Rco_{pLS20}-mediated repression of the P_c promoter. Importantly, as for Phr^*_{pLS20}, colonies were white in the presence of each of the other three peptides, strongly indicating that they also inhibited the activity of Rap_{pLS20} *in vivo*. In line with the AUC *in vitro* results presented above, different concentrations of the peptides were required to inactivate Rap_{pLS20}. While 10 μM of Phr^*_{pLS20} was sufficient to obtain white colonies, 60 μM of PhrF*-R2K and PhrF*-I5Y and 120 μM of PhrF* were required to obtain the same result. Most likely, this is due to the different affinities of PhrF* and the variants for Rap_{pLS20} as observed *in vitro*.

Relative strengths of promoters involved in regulating conjugation

In a previous study we demonstrated, using transcriptional *lacZ* fusions, that the main conjugation promoter P_c is a strong promoter, and that the divergently oriented and overlapping P_r promoter driving expression of rco_{pLS20} is a very weak promoter whose activity was not detected without the expression of its activator rco_{pLS20} (34). More recently, we have constructed a promoter screening system based on fusions with a *gfp* reporter gene which is more sensitive and versatile than the *lacZ*-based system, and allows promoter activity determination in individual cells (43). In that study, we confirmed that P_c is a strong promoter (strain AND2A). To obtain a more comprehensive understanding of the relative strengths of the different promoters encoding the players involved in regulation of the conjugation genes, we used this *gfp*-based promoter-screening system to construct strains containing transcriptional *gfp* fusions with the P_r and the P_{rap} promoters. Based on the following reasoning

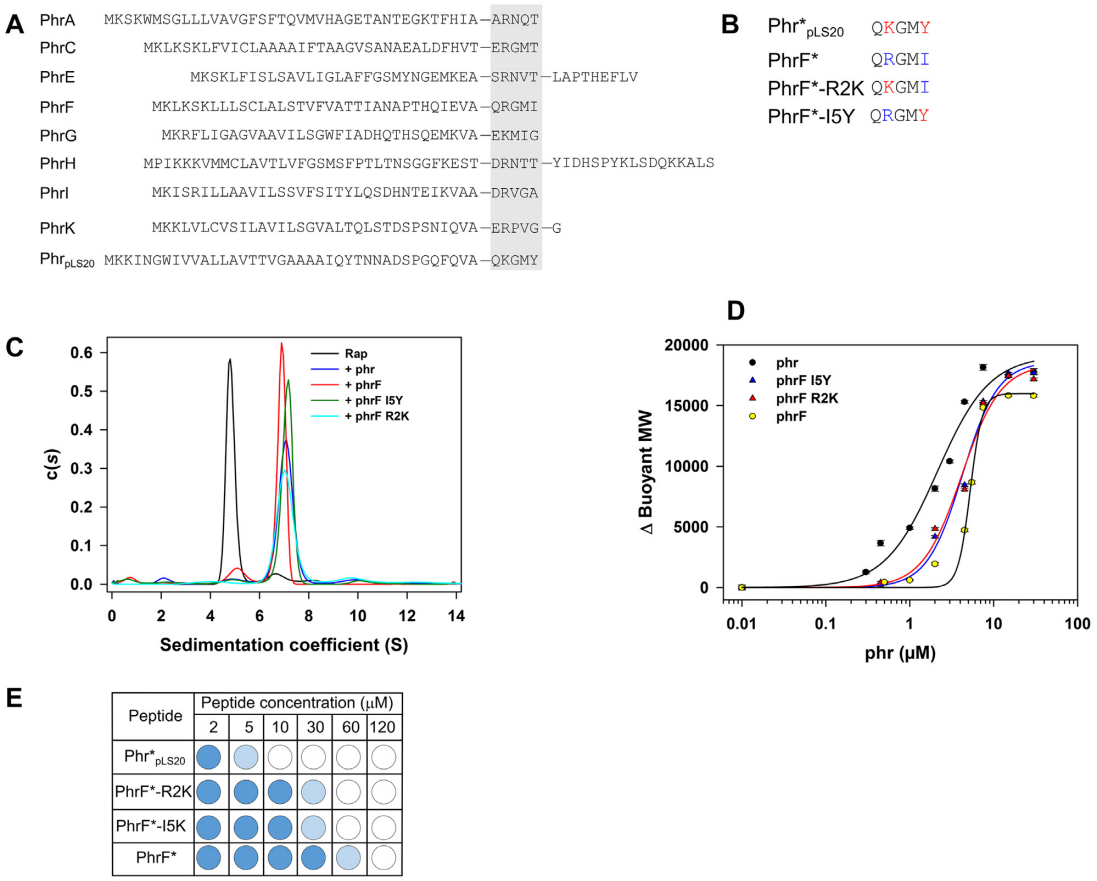

Figure 2. *B. subtilis* genome encoded PhrF* and the peptide variants PhrF*-R2K and PhrF*-I5Y can interact with Rap_{pLS20} *in vitro* and *in vivo*. (**A**) Four of the five residues of mature Phr peptides Phr^*_{pLS20} and PhrF* are conserved. Alignment of the Phr peptides encoded by the *B. subtilis* genome and by pLS20. The mature peptides are indicated with a grey background. (**B**) Sequences of the mature Phr^*_{pLS20} and PhrF* peptides, and the peptide variants PhrF*-R2K and PhrF*-I5Y. The deviant residues at positions 2 and 5 are indicated in red in Phr^*_{pLS20} and blue in PhrF*. This red/blue colour code is also in the peptide variants if their position corresponds to that present in Phr^*_{pLS20} or PhrF*. (**C**) PhrF* and its peptide variants PhrF*-R2K and PhrF*-I5Y can induce Rap_{pLS20} tetramerization. Sedimentation coefficient distribution, c(s), corresponding to 4.5 μM Rap_{pLS20} alone (black trace), or with 45 μM of Phr^*_{pLS20} (blue trace), PhrF* (red trace), PhrF*-I5Y (green trace) and PhrF*-R2K (cyan trace). (**D**) Binding isotherms for the interaction of Rap_{pLS20} with Phr^*_{pLS20} (black circles), PhrF* (yellow circles), PhrF*-I5Y (blue triangles) and PhrF*-R2K (red triangles). The solid curves represent the best fit of the three-parameters Hill equation to the SE experimental data. (**E**) The mature PhrF* and its variants PhrF*-R2K and PhrF*-I5Y can inhibit Rap_{pLS20} *in vivo*. Cells of *B. subtilis* strain PKS25 (*thrC*::P_c-*lacZ, amyE*::P_{spank}-rco_{pLS20}, *lacA*::P_{xyl}-rap_{pLS20}) were plated onto plates containing Xgal, IPTG (10 μM) and xylose (1%), and supplemented with the indicated concentration of Phr^*_{pLS20}, PhrF*, PhrF*-R2K or PhrF*-I5Y. Plates were screened for colour after overnight incubation at 37°C (see Supplemental Figure S3 for original colonies).

we tested also the possibility that phr_{pLS20} may be preceded by a promoter. rap_{pLS20} and phr_{pLS20} are transcriptionally coupled (stop codon of rap_{pLS20} overlaps with the phr_{pLS20} start codon) and, hence, are both under the control of a promoter P_{rap}. After transcription and translation, synthesized Rap_{pLS20} remains inside the cell but the small Phr_{pLS20} is secreted and therefore its concentration will drop. For proper functioning of the quorum sensing system, one might expect that the expression level of phr_{pLS20} would be higher than that of rap_{pLS20}. This could be achieved if phr_{pLS20} is expressed, besides P_{rap}, from an additional promoter. To test this possibility, we constructed strain AL21 in which the region upstream of phr_{pLS20} was cloned in front of the *gfp* gene. FACS analysis using standard conditions (see Materials and Methods) was used to determine the fluorescence level of AL21 cells as well as the control strains containing the *gfp* gene fused to the relatively strong and very strong IPTG-inducible promoters P_{spank} and $P_{hyperspank}$, respectively, grown in the presence of 1 mM IPTG.

Of the pLS20 promoters tested, P_c was the strongest (see Figure 3). In line with our previous results, its strength was similar to that of the $P_{hyspank}$ promoter induced in the presence of 1 mM IPTG (see Figure 3 and reference 43). The fluorescence level dropped ∼20-fold in the presence of pLS20spec (strain AND2A_P) due to repression of P_c by Rco_{pLS20} synthesized by the plasmid (see below). A very low promoter activity, barely above background levels, was observed for promoter P_r when tested in the absence of pLS20. In the presence of pLS20spec, clear fluorescence levels were detected but the promoter activity was still very low, confirming that P_r is a weak promoter even when activated by Rco_{pLS20}. Analysis of strain GR152 showed that P_{rap} controlling expression of rap_{pLS20} and phr_{pLS20} was also a weak promoter. Interestingly, promoter activity with a strength

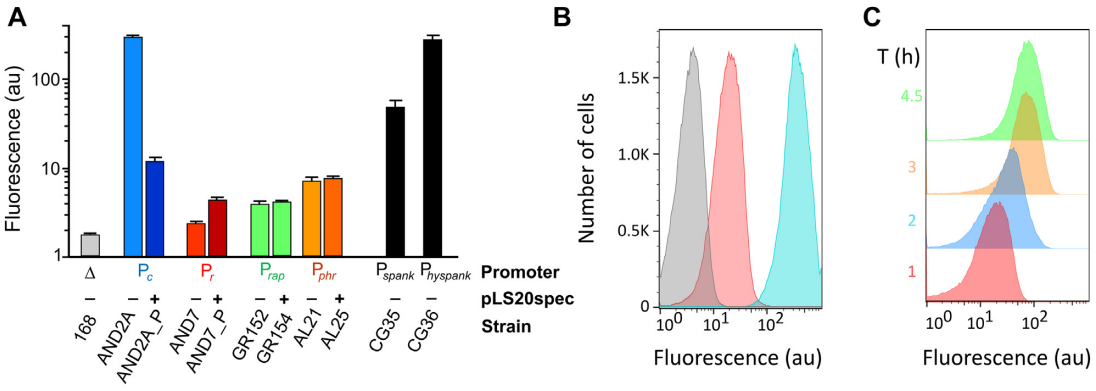

Figure 3. Flow cytometry analyses to determine relative promoter strengths and the activity of promoter P_c at population level. (**A**) Relative promoter strengths determined by flow cytometry using strains containing promoter P_c, P_r, P_{rap} or P_{phr} transcriptionally fused to *gfp*. A negative control strain and positive control strains containing *gfp* fused to the IPTG-inducible promoter P_{spank} or $P_{hyspank}$ were included. Samples withdrawn from late exponentially growing cultures (OD_{600} between 0.8 and 1) were analysed by FACS. At least 100 000 cells were analysed for each sample. Colour codes: grey, negative control strain 168; black, control strains containing the IPTG-inducible P_{spank} (strain CG35) or $P_{hyspank}$ (strains CG36) fused to the *gfp* gene (grown in the presence of 1 mM IPTG); blue, red, green and brown, strains containing *gfp* fused to promoters P_c, P_r, P_{rap} and P_{phr}, respectively. Light and dark coloured bars reflect strains lacking and containing pLS20spec, respectively. Names of the strains are given below the graphic. For each strain, the mean values of geomean determinations of at least three independent FACS analyses are given together with their standard deviations. (**B, C**) Homogeneous expression of P_c-*gfp* in strains containing or lacking pLS20. (**B**) Samples of cultures of AND2A (*amyE*::P_c-*gfp,* blue pattern), AND2A_P (*amyE*::P_c-*gfp*, pLS20spec, red pattern) or PKS89 (*amyE*::promoterless *gfp*, grey pattern) cells, collected at $OD_{600} = 1$, were subjected to flow cytometry analysis. (**C**) An overnight grown culture of strain *B. subtilis* 168 strain harbouring pLS20gfp28 (strain PKS182) was diluted 100-fold in fresh prewarmed LB medium. Next, samples were taken at the indicated times and analysed by flow cytometry.

almost double that of promoter P_{rap} was observed for strain AL21. This demonstrates that phr_{pLS20} is controlled by an additional promoter, i.e. expression of phr_{pLS20} is controlled by promoters P_{rap} and P_{phr}. Finally, contrary to that of P_c and P_r, similar activities of promoters P_{rap} and P_{phr} were observed regardless whether the strains contained pLS20spec (Figure 3), indicating that Rco_{pLS20} does not regulate the activity of these two promoters.

Computer-assisted and manual analyses of the cloned DNA regions preceding rap_{pLS20} and phr_{pLS20} were performed to identify the putative promoters P_{rap} and P_{phr}. This resulted in the identification of sequences that shared similarities with the consensus sequence of σ^A-dependent promoters (5′-TTGACA-17/18bp-TATAAT-3′). In the case of rap_{pLS20} and phr_{pLS20} these sequences correspond to 5′-ttcgt**TTGAtA**-gacattagtattttaata-**TATttT**-tcctg-3′ and 5′-atgcc**TTGACt**-gaggccttggatcatggc **TATgAT**-aagcc-3′ (putative −35 and −10 hexamer sequences indicated in bold), respectively. The following data provided evidence that the identified sequences corresponded to promoters P_{rap} and P_{phr}. Previously, we have published a heatmap expression profile of pLS20cat based on RNAseq of pLS20cat-containing cells harvested at the end of the exponential growth phase, also the highest conjugation state (27). We reassessed this data and instead of a heatmap we now plotted the expression levels along the plasmid genome for the region spanning rap_{pLS20} and phr_{pLS20}. The plot in Supplemental Figure S4 shows that phr_{pLS20} is indeed expressed at higher levels than rap_{pLS20}. In addition, the positions of the putative P_{rap} and P_{phr} promoters identified based on similarity with σ^A consensus sequences correspond with the approximate starting positions of expression upstream of rap_{pLS20}, and that of the increased levels starting upstream of phr_{pLS20} observed in RNAseq.

The P_c promoter is homogeneously expressed

GFP-based transcriptional fusions allow quantification of the relative promoter activity at single cell level. In addition, heterogeneous or bimodal expression of any particular gene in the population is easily visualized. We used this approach to study if the multi-layered regulation of the P_c promoter including the Rap/Phr-based quorum sensing mechanism (34) resulted in heterogeneous activity of promoter P_c. Thus, samples taken from cultures of AND2A cells (*amyE*::P_c-*gfp*), AND2A-P cells (*amyE*::P_c-*gfp*, pLS20spec) and the control strain PKS89 (*amyE*::promoterless-*gfp*) at $OD_{600} = 1$, when conjugation efficiencies are at their maximum (27), were analysed by flow cytometry. The results presented in Figure 3B show a homogeneous activity of P_c irrespective of the presence or absence of pLS20spec. The lower fluorescence levels in AND2A_P are the consequence of the P_c promoter being activated for a shorter time as compared to the constitutively active P_c promoter in AND2A. In this set up, the activity of the P_c promoter was analysed using an ectopic copy of the promoter located on the bacterial chromosome whereas the proteins regulating its activity are encoded by the resident plasmid, which itself also contains a copy of the P_c promoter. Several factors might affect proper regulation of the uncoupled and ectopically located P_c promoter such as differences in local supercoiling or spatial location, or the absence of coupled transcription and translation. We therefore constructed a derivative of pLS20cat, pLS20gfp28, in which a copy of the *gfp* gene was placed behind the first gene of the conjugation operon (gene *28*). Strain PKS182 harbouring pLS20gfp28 was then used to determine the fluorescence distribution pattern at single cell level in the population as a function of growth. Thus, on the one hand, samples taken at different times from a growing culture were analysed by flow cytometry, and on the other

hand, time-lapse microscopy was used to visualize the fluorescence distribution in a growing microcolony. The results shown in Figure 3C and Supplemental Figure S5 revealed a homogenous pattern of P_c promoter activity in this set up. Both approaches show that most cells started to display a rather uniform level of fluorescence whose intensity first increased in time and at later stages declined in a rather uniform manner. Together, these results provide compelling evidence that the different layers of regulation acting on the P_c promoter result in a sensitive genetic switch that transiently activates the P_c promoter in a coordinated manner in most or all pLS20-containing cells.

Rap_{pLS20} is not a DNA binding protein and does not activate the P_c promoter by competing with Rco_{pLS20} for binding to the Rco_{pLS20} operator sites

The results presented above show that Rap_{pLS20} is sufficient to relieve Rco_{pLS20}-mediated repression of the P_c promoter. Rap_{pLS20} belongs to the RRNPP family of proteins. Many RRNPP members regulate transcription by binding to DNA (see Introduction). It was therefore not unlikely that Rap_{pLS20} could be a DNA binding protein and that it exerts its anti-repressive activity by competing with Rco_{pLS20} for binding to the same DNA motif. We tested this possibility by Electrophoretic Mobility Shift Assays (EMSA) using a purified C-terminal His tagged version (referred to here as Rap_{pLS20} for simplicity), which –contrary to an N-terminal His tagged version- was functional *in vivo* (see Materials and Methods and Supplemental Table S3). However, purified Rap_{pLS20} was not able to bind a 186 bp DNA fragment encompassing an Rco_{pLS20} binding site (operator O_I) (see Supplemental Figure S6). This was contrary to Rco_{pLS20} (see below) which was able to bind this DNA fragment. These results indicate that Rap_{pLS20} is not a DNA binding protein and that it is unlikely therefore, that it exerts its antirepressive effect by competing with Rco_{pLS20} for the same DNA binding site.

Evidence for homogeneous and heterogeneous interactions between Rap_{pLS20} and Rco_{pLS20} *in vivo*

Another possibility of how Rap_{pLS20} might relieve Rco_{pLS20}-mediated repression of the P_c is through direct interaction with Rco_{pLS20}. Possible interaction between Rap_{pLS20} and Rco_{pLS20} was tested *in vivo* and *in vitro*. For the *in vivo* approach we used the bacterial two-hybrid system (B2HS). For this, rap_{pLS20} and rco_{pLS20} were fused in frame at the 5′ and 3′ regions encoding the T18 or T25 fragments of adenylate cyclase, and combinations of the resulting plasmids were co-transformed into *E. coli* BTH101 and plated onto M63 agar plates supplemented with maltose, Xgal and IPTG. A schematic presentation of the fusion genes constructed is shown in Supplemental Figure S7 and relevant crosses are presented in Figure 4A. As expected, whereas negative controls did not give colonies, positive controls resulted in the appearance of blue colonies. Interestingly, blue colonies were also obtained for two crosses, *T25rap/rcoT18* and *T18rap/T25rco*, indicating that Rap_{pLS20} and Rco_{pLS20} interact *in vivo*. Another cross, *rapT25/T18rco*, did not show a positive interaction possibly because the linkers and the positions of the fusions prevented the interaction. Because these experiments were performed in the heterologous host *E. coli*, the results obtained imply that interaction between Rap_{pLS20} and Rco_{pLS20} do not require other pLS20- or *B. subtilis*-encoded proteins.

Taking advantage of the vectors constructed, we used the B2HS also to test possible self-interactions of Rap_{pLS20} and Rco_{pLS20}. As shown in Figure 4A, different crosses of T18 and T25 genes fused to either rap_{pLS20} or rco_{pLS20} also resulted in the appearance of blue colonies, indicating that both Rap_{pLS20} and Rco_{pLS20} self-interact. These *in vivo* results corroborate our previously published analytical ultracentrifugation results demonstrating that Rco_{pLS20} forms tetramers in solution (34), and that Rap_{pLS20} forms dimers in solution (42).

Rap_{pLS20} and Rco_{pLS20} interact *in vitro*

Possible interaction between Rap_{pLS20} dimers and Rco_{pLS20} tetramers was studied by sedimentation velocity (SV). Rap_{pLS20} at 4.5 μM was titrated with different Rco_{pLS20} concentrations ranging from 0.6 to 27.0 μM. Analysis of the mixtures displayed the presence of three new peaks at higher sedimentation coefficient than the Rap_{pLS20} dimers and Rco_{pLS20} tetramers alone, corresponding to Rap_{pLS20}–Rco_{pLS20} complexes. As shown in Figure 4B, Rap_{pLS20} dimers interacted directly with Rco_{pLS20} tetramers *in vitro* to form a species at 7.1S that, once corrected to standard conditions ($s_{20,w} = 7.7S$), is compatible with the theoretical mass of a nearly globular ($f/f_0 = 1.36$) complex made of one Rap_{pLS20} dimer and one Rco_{pLS20} tetramer. Besides this predominant complex, minor amounts of species with higher sedimentation coefficients of 11.3*S* and 14.2*S* were observed, corresponding to undefined higher oligomerization complexes.

To fully extract the maximum information enclosed in the SV data, besides the hydrodynamic separation of the complexes, we took advantage of the simultaneous absorbance data acquisition at 250 and 280 nm and globally analysed them through SEDPHAT to get the diffusion-deconvoluted sedimentation coefficient distributions with spectral deconvolution of the absorbance signals, $c_k(s)$ (Figure 4C). Further improvement of the molar ratio resolution was achieved by using both, mass conservation constraint and multi-segmented model restriction, using our prior knowledge that, once mixed, Rap_{pLS20} at 4.5 μM reacts fully with Rco_{pLS20} at 25 μM and no free Rap_{pLS20} sediments in the low-*s* region from 0.1*S* to 6*S*. The MSSV analysis of the Rco_{pLS20}–Rap_{pLS20} complex sedimenting at 7.1S indicated that the areas under the peak corresponded to a stoichiometry of 2.1 mol of Rco_{pLS20} per mol of Rap_{pLS20}. This result was in tune with the above mentioned putative complex composition involving one Rco_{pLS20} tetramer bound to one Rap_{pLS20} dimer, deduced from the hydrodynamic behavior observed in the previous SV assay.

Binding of Rco_{pLS20} to a DNA fragment encompassing operators O_I and O_{II}

The intergenic region between rco_{pLS20} and gene *28*, which contains Rco_{pLS20} operators O_I and O_{II}, is intrinsically bent

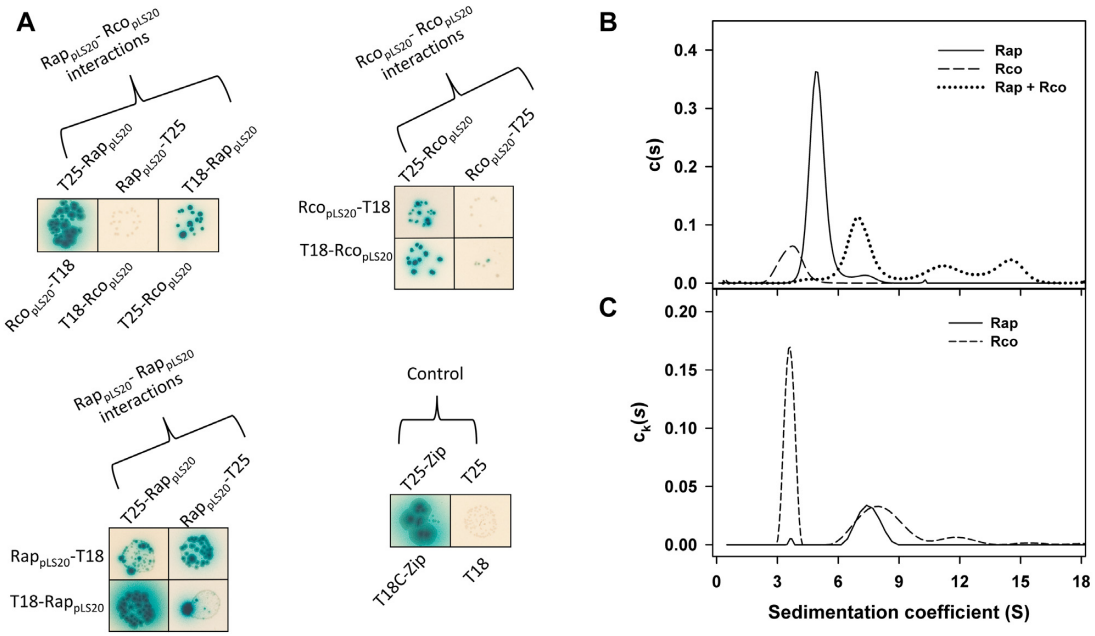

Figure 4. Interaction of Rap_{pLS20} and Rco_{pLS20} shown by *in vivo* and *in vitro* approaches. (**A**) *In vivo* bacterial two hybrid system analyses to study homo and heterogeneic interactions between Rap_{pLS20} and Rco_{pLS20}. In-frame translational fusions were constructed with the N-terminal (T25) and C-terminal (T18) regions of the catalytic domain of the *Bordetella pertussis* adenylate cyclase (*cya*) gene (see Materials and Methods) resulting in vectors pEST1 to pEST8. Combinations of these vectors (crosses) were used to transform competent *E. coli* BTH101, and dilutions were subsequently spotted onto M63 plates supplemented with maltose, IPTG and Xgal. Functional complementation of the T25 and T18 fragments can occur when the proteins fused to these fragments interact with each other, resulting in indirect activation of the *lac* and *mal* operons, which then allows growth of the *E. coli* cells, resulting in the appearance of blue colonies when plated on M63 plates supplemented with maltose, IPTG and Xgal. In other words, appearance of blue colonies indicate interaction of the protein moieties fused to the T25 and T18 fragments. Other possible crosses gave negative results (not shown). Relevant crosses are indicated. Names of the fusion proteins are shown. The panels show crosses to study interactions between (Rap_{pLS20} and Rco_{pLS20}), self-interactions between Rco_{pLS20}, self-interactions between Rap_{pLS20}, and positive and negative controls. Positive control, crosses between vectors pKT25-zip and pUT18C-Zip, containing fusions with the leucine zipper of GCN4. Negative control, vectors lacking an in frame fusions. (B, C) Rap_{pLS20} and Rco_{pLS20} interact *in vitro*. (**B**) Sedimentation velocity assay at 280 nm showing the sedimentation coefficient distribution c(s) corresponding to Rco_{pLS20} at 9 μM (dashed line), Rap_{pLS20} at 4.5 μM (black line), and the mixture of both proteins at those concentrations (dotted line). (**C**) Global multiwavelength (250 and 280 nm) analysis of Rap_{pLS20}-Rco_{pLS20} complexes and decomposition into component sedimentation coefficient distributions, $c_k(s)$, for Rap_{pLS20} (solid trace) and Rco_{pLS20} (dashed trace).

(34). Binding of Rco_{pLS20} to its operators O_I and O_{II} results in looping of the 75 bp spacer region and this looped configuration is required for proper regulation of the P_c and P_r promoters (34, see also Introduction). Previous EMSAs showed that binding of Rco_{pLS20} to a 392 bp DNA fragment encompassing operators O_I and O_{II}, named Fragment V (FV, see Figure 5A), resulted in the appearance of up to four retarded species, depending on the concentration of Rco_{pLS20} (34). The results presented above show that Rap_{pLS20} interacts with Rco_{pLS20}. However, it is not clear whether Rap_{pLS20} can interact with Rco_{pLS20} when bound to DNA, and how Rap_{pLS20} inhibits the transcriptional regulatory activities of Rco_{pLS20}. We used AUC (described here) and biochemical approaches (described below) to gain insight into the mechanism by which Rap_{pLS20} relieves Rco_{pLS20}-mediated repression of the P_c promoter. In a first experiment, we used fragment FV, encompassing Rco_{pLS20} operators O_I and O_{II} (see Figure 5A), to test possible effects of Rap_{pLS20} on the DNA binding activity of Rco_{pLS20}. Samples of DNA fragment FV in the absence or presence of different concentrations of Rco_{pLS20} were analysed by SV at 260 nm to track DNA. Increasing Rco_{pLS20} concentrations resulted in highly polydispersed sedimentation coefficient distributions, suggesting that, as observed in gel retardation assays, multiple nucleoprotein complexes were formed (see Supplemental Figure S8). The polydispersity of the complexes made it extremely difficult to analyse them in further detail. However, a striking result was that in the presence of Rap_{pLS20} the species with the highest sedimentation coefficient (ranging from 20*S* to 35*S*), probably corresponding to looped DNA–Rco_{pLS20} complexes, disappeared. Control SV experiments showed that no DNA binding of Rap_{pLS20} to DNA fragment FV was observed (not shown), in agreement with the EMSA result described above (Supplemental Figure S6). Moreover, the addition of Rap_{pLS20} did not result in formation of DNA-protein complexes with increased sedimentation coefficient compared to those observed in the presence of only Rco_{pLS20} (Supplemental Figure S8). This strongly indicates that Rap_{pLS20} did not form stable DNA-Rco_{pLS20}-Rap_{pLS20} complexes. Rather, it suggests that Rap_{pLS20} affects the DNA binding activity of Rco_{pLS20}.

Rco_{pLS20} bridges two DNA fragments containing operator O_{II}

The results presented above show that Rap_{pLS20} preferentially acted on high molecular weight Rco_{pLS20}–DNA com-

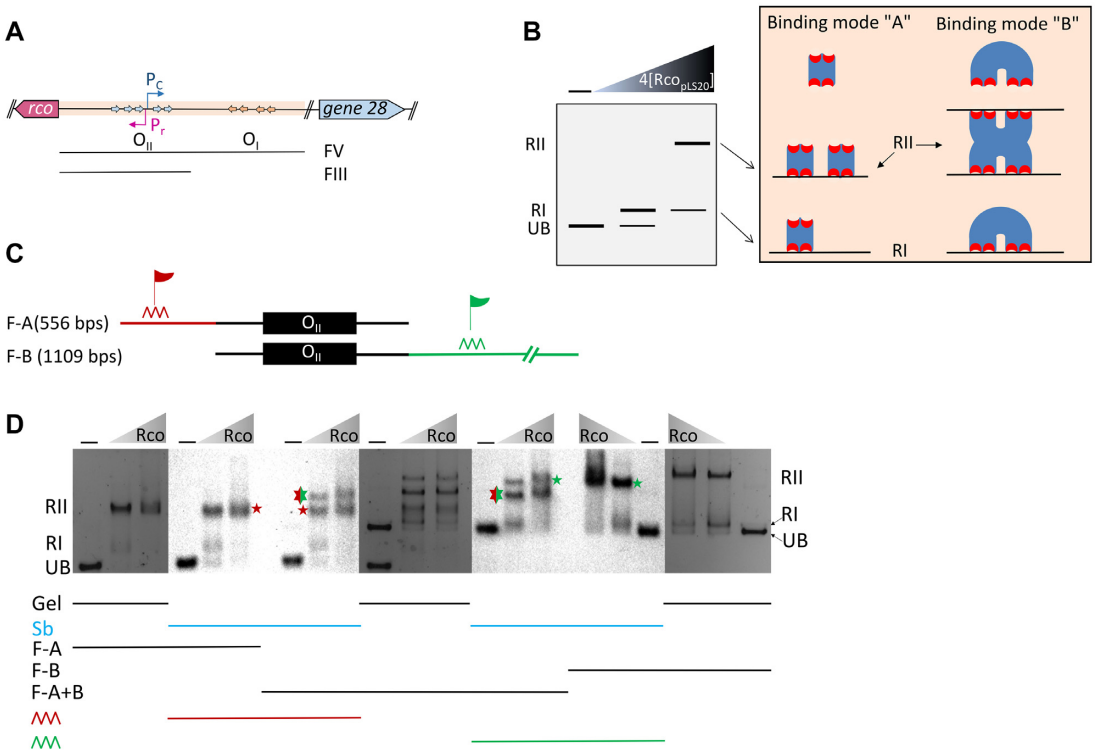

Figure 5. Rco$_{pLS20}$ bridges two DNA molecules containing an Rco$_{pLS20}$ operator. (**A**) Upper panel: schematic view of the intergenic *rco$_{pLS20}$*-gene *28* region on pLS20 and the positions of Rco$_{pLS20}$ operators O_I and O_{II} that are separated by 75 bp. Lower panel: indications of fragments FV and FIII containing both or only operator O_{II}, respectively. (**B**) Schematic representation of possible binding modes of Rco$_{pLS20}$ tetramers to DNA fragment encompassing one Rco$_{pLS20}$ operator. Left panel, representation of two retarded species observed in gel retardation assays using a DNA fragment containing either operator O_I or O_{II}. UB, unbound DNA, RI, retarded species I, RII, retarded species II. Right panel, two different ways of how Rco$_{pLS20}$ tetramers may bind to the DNA fragment. In binding mode 'A' one DNA fragment would be able to bind a maximum of two Rco$_{pLS20}$ tetramers. One and two Rco$_{pLS20}$ tetramers would be bound to species RI and RII, respectively. In binding mode 'B' only one Rco$_{pLS20}$ tetramer can bind to a DNA molecule, corresponding to retarded species RI. Retarded species RII would correspond to a sandwiched configuration in which two DNA molecules are bridged through interactions between Rco$_{pLS20}$ tetramers bound to either DNA molecule. (**C**) Schematic representation of the DNA fragments used for gel retardation and subsequent Southern blotting. Both DNA fragments contain Rco$_{pLS20}$ operator O_{II} (black rectangle) but have a different size and have unique sequences located at the 5′ side (small DNA fragment [556 bp], indicated with red line) or the 3′ side of the O_{II} operator (large DNA fragment [1,109] bp, indicated with green line). The approximate DNA sequences used for generating probes specific for these unique flanking sequences are indicated with teeth like and flag symbols. (**D**) EMSA and Southern blot results of individual fragment F-A or F-B, and of fragments F-A and F-B together. DNA fragments were run on an agarose gel either without or in the presence of 3.4 or 6.8 μM of Rco$_{pLS20}$. After running, the gel was stained with ethidium bromide and photographed. Migrating positions of free DNA and the retarded species (RI and RII) are indicated. In addition, in the Southern blots retarded RII species of the small and large DNA fragment are indicated with a red and green asterisk, respectively. The red-and-green asterisk indicate the additional retarded species that is observed only when the reaction mixture contained both the large and the small DNA fragment. This retarded species, which migrated in between the positions of the retarded species RII of the small and the large DNA fragment, hybridized with probes specific for both of these fragments. A duplicate gel was used for a Southern blot that was hybridized first with a probe specific for the small fragment and after stripping the same blot was used for hybridization with a probe specific for the large DNA fragment. The horizontal lines in the lower part indicate which panels correspond to the stained gels (gel) and Southern blots (Sb, blue line), what fragment was used (F-A, F-B or [F-A + F-B]), and what probe was used; red and green teeth-like symbol for the small and large DNA fragment, respectively.

plexes, suggesting that the nature of these complexes is fundamentally different from the lower molecular weight Rco$_{pLS20}$–DNA complexes. One attractive possibility is that the high molecular weight Rco$_{pLS20}$–DNA complexes correspond to looped DNA molecules. However, in this set up it is hard to determine the nature of these high molecular weight complexes due to the presence of multiple Rco$_{pLS20}$-DNA species. Hence, we searched for a simpler experimental set up involving Rco$_{pLS20}$-mediated loop formation. In previous work, we showed that gel retardation experiments gave very similar results for the ∼180 bp fragments containing only the Rco$_{pLS20}$ operator O_I or operator O_{II}. In both cases, a maximum of two retarded species were observed depending on the concentration of Rco$_{pLS20}$. At very low Rco$_{pLS20}$ concentrations only one retarded species (named Retarded Species I, RI) was observed, but an additional slower migrating species, (named Retarded species II, RII) was observed at increasing Rco$_{pLS20}$ concentrations, which became the predominant retarded species at high Rco$_{pLS20}$ concentrations (34). At the time, we postulated that these results could reflect cooperative binding of two Rco$_{pLS20}$ tetramers to one DNA molecule containing an Rco$_{pLS20}$ operator (see Figure 5B for a schematic view). If Rco$_{pLS20}$ binds DNA in this mode, then the Helix-Turn-Helix domain of two of the four Rco$_{pLS20}$ monomers of each Rco$_{pLS20}$-tetramer would not be bound to the DNA molecule and hence would be available to bind other DNA molecule(s), which would result in the generation of more than two re-

tarded species (Figure 5B, binding mode 'A'). An alternative mode of DNA binding that explains a maximum of only two retarded species would be that only one Rco_{pLS20} tetramer is able to bind to a DNA molecule containing a single operator resulting in the fastest migrating retarded species RI. Retarded species RII would then be the result of two DNA molecules that are bridged through interactions of the Rco_{pLS20} tetramers bound to each DNA molecule (Figure 5B, binding mode 'B'). This situation would be similar to that of a DNA looped configuration and, if correct, this would be an ideal system to test if Rap_{pLS20} preferentially acts on DNA-looped structures.

We therefore used the approach schematically presented in Figure 5C to test if the retarded RII species observed in EMSA corresponded to two DNA molecules bridged by Rco_{pLS20}. In short, two DNA fragments were generated having an overlapping region that contains Rco_{pLS20} operator O_{II}. The fragments were different in size and the regions flanking the operator were unique in each fragment, allowing the fragments to be distinguished in Southern blotting experiments using fragment-specific probes. When analysed separately in gel retardation experiments in the presence of Rco_{pLS20}, each DNA fragment was expected to give two retarded species, although their migration position would be distinct due to the different sizes of the fragments. When using samples containing both DNA fragments, it was expected that the retarded species migrate to the same positions as observed when each DNA fragment was analysed alone. However, if the RII species corresponded to two DNA molecules bridged by two Rco_{pLS20} tetramers, an additional retarded species, corresponding to a complex of a large and a short DNA molecule, would be expected. This additional retarded species would migrate in between the positions observed for the retarded RII species formed by the two small or two large DNA molecules. If such an additional species was present, Southern blotting using probes specific for each DNA fragments could demonstrate the presence of both the short and large DNA fragment in this retarded species.

The results of this experiment, which are presented in Figure 5D, show indeed the presence of an additional retarded species that migrated in between the positions of retarded species RII formed by the two small and two large DNA fragments, and which hybridized to both probes specific to the small and the large DNA fragments, consistent with the two DNA molecules being bridged by Rco_{pLS20} tetramers bound to either DNA molecule.

To confirm these data by an independent approach, we took advantage of the stoichiometry determination of DNA-protein complexes by multi-signal sedimentation velocity (MSSV) (44). Thus, SV experiments were performed using samples containing the 219 bp DNA fragment FIII (encompassing Rco_{pLS20} operator O_{II}) alone or with increasing Rco_{pLS20} concentrations. Absorbance data at 260 and 280 nm were simultaneously collected and globally analysed through SEDPHAT to obtain the diffusion-deconvoluted sedimentation coefficient distributions with spectral deconvolution of the absorbance signals, $c_k(s)$ besides the hydrodynamic separation of the complexes. Sedimentation velocity titration of fragment FIII at 140 nM

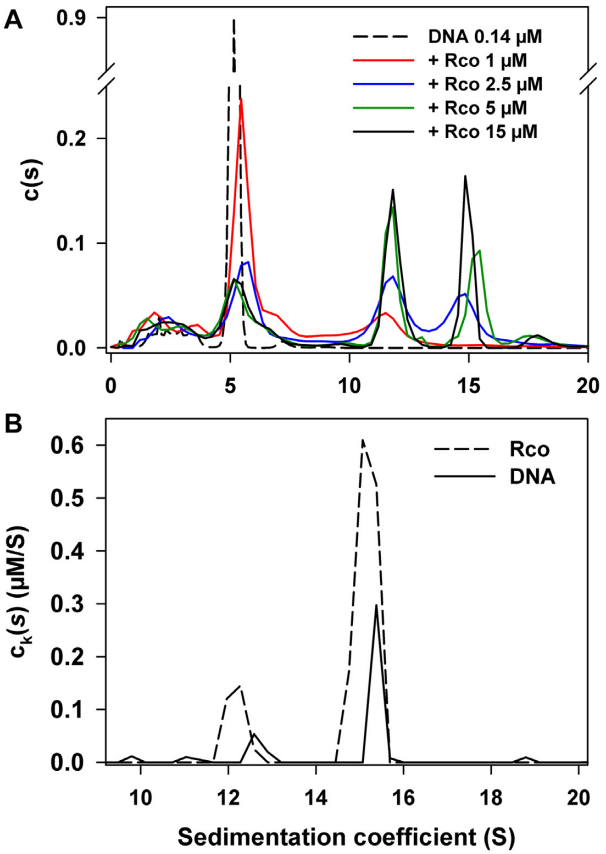

Figure 6. Rco_{pLS20} binds DNA fragment FIII leading to two different complexes. (**A**) Sedimentation coefficient distribution, $c(s)$, obtained by SV at 260 nm of 140 nM DNA fragment FIII alone (dashed trace), or incubated with increasing Rco_{pLS20} concentrations: 1 μM (red trace), 2.5 μM (blue trace), 5 μM (green trace) and 15 μM (black trace). (**B**) Global multiwavelength (260 and 280 nm) analysis of Rco_{pLS20}–DNA fragment III complexes and decomposition into component sedimentation coefficient distributions, $c_k(s)$, for Rco_{pLS20} (dashed trace) and the DNA fragment III (solid trace). For clarity, when comparing the areas under the peaks ascribed to the complexes the low-s range where only Rco_{pLS20} and DNA fragment FIII sediment is not shown.

with Rco_{pLS20} (1–15 μM) showed the presence of two species with higher sedimentation coefficient than DNA or protein alone, pointing to the formation of two different Rco_{pLS20}–DNA complexes, in line with the results obtained by gel retardation. At the lowest Rco_{pLS20} concentration assayed (1 μM) only a species sedimenting at 11.8S ($s_{20,w}$ = 12.9 S) was observed, whereas from 2.5 μM the second species at 14.9S ($s_{20,w}$ = 16.3 S) appeared and the amount of both complexes gradually increased (Figure 6A). The MSSV analysis of Rco_{pLS20}-fragment FIII complexes indicated that the areas under the peaks at 11.8S and 14.9S corresponded to a stoichiometry of 3.9 and 4.3 mol of Rco_{pLS20} bound per mol of DNA fragment FIII, respectively (Figure 6B). This stoichiometry perfectly matches the deduced composition by EMSA consisting of one Rco_{pLS20} tetramer bound to one DNA molecule and two DNA molecules being bridged by two Rco_{pLS20} tetramers for RI and RII, respectively.

Rap_{pLS20} preferentially acts on Rco_{pLS20} oligomers involved in DNA looping

The results presented above demonstrate that two Rco_{pLS20}–DNA complexes were formed upon interaction of Rco_{pLS20} with a DNA fragment comprising only one Rco_{pLS20} operator, and that the retarded species RII observed in gel retardation experiments, or the peak at 14.9*S* observed by SV, corresponded to two DNA molecules being bridged by two Rco_{pLS20} tetramers. Thus, we used this experimental set up applying the DNA fragment containing operator O_{II} (DNA fragment FIII, 219 bp) to assess the effects of Rap_{pLS20} on the two different Rco_{pLS20}–DNA complexes by two independent techniques: AUC and gel retardation, whose different underlying principles make them interesting complementary approaches. Using EMSA, we were able to establish conditions in which a certain concentration of Rco_{pLS20} (0.25 μM) resulted in the appearance of only retarded species RI, whereas a four-fold higher concentration of Rco_{pLS20} resulted in the appearance of retardation species RI and RII (see Supplemental Figure S9). These conditions were used in the gel retardation experiments shown in Figure 7A. Addition of low concentrations of Rap_{pLS20} to pre-incubated mixtures of Rco_{pLS20} and DNA, which in the absence of Rap_{pLS20} formed two types of Rco_{pLS20}–DNA complexes (i.e. retarded species RI and RII) in gel retardation studies, resulted in the specific removal of species RII in a concentration-dependent manner (Figure 7A) without affecting the retarded species RI (right panel). A similar effect was observed by SV assays at 260 nm, where a pre-incubated mixture of DNA fragment FIII (140 nM) and Rco_{pLS20} at 2.5 μM was titrated with increasing concentrations of Rap_{pLS20} (5–15 μM). The addition of increasing concentrations of Rap_{pLS20} down-modulated the formation of the two Rco_{pLS20}–DNA complexes at 11.8*S* and 14.9*S* observed in the absence of Rap_{pLS20}, hence the interaction of Rco_{pLS20} with DNA fragment FIII (Figure 7B). These results indicate that Rap_{pLS20} is able to interact with Rco_{pLS20} bound to DNA and that this binding results in the release of Rco_{pLS20} from the DNA, as demonstrated by the gradual increase of free DNA at 5.0*S* when increasing the concentration of Rap_{pLS20}. Interestingly, when the SV assay was performed at 230 nm to enhance absorbance signal from the proteins, addition of Rap_{pLS20} at 25 μM to the pre-incubated DNA Rco_{pLS20} mixture showed the removal of Rco_{pLS20} from the Rco_{pLS20}-DNA complexes to form free DNA and the 7.1S Rap_{pLS20}–Rco_{pLS20} complex (Figure 7B). This shows that Rap_{pLS20} is not only able to detach Rco_{pLS20} from DNA fragment FIII but to bind to Rco_{pLS20} to form a steady protein complex. Furthermore, particularly at 25 μM, Rap_{pLS20} acted preferentially on Rco_{pLS20}–DNA complexes having the highest sedimentation coefficient, in tune with the preferential interaction of Rap_{pLS20} with retarded species RII observed in EMSA.

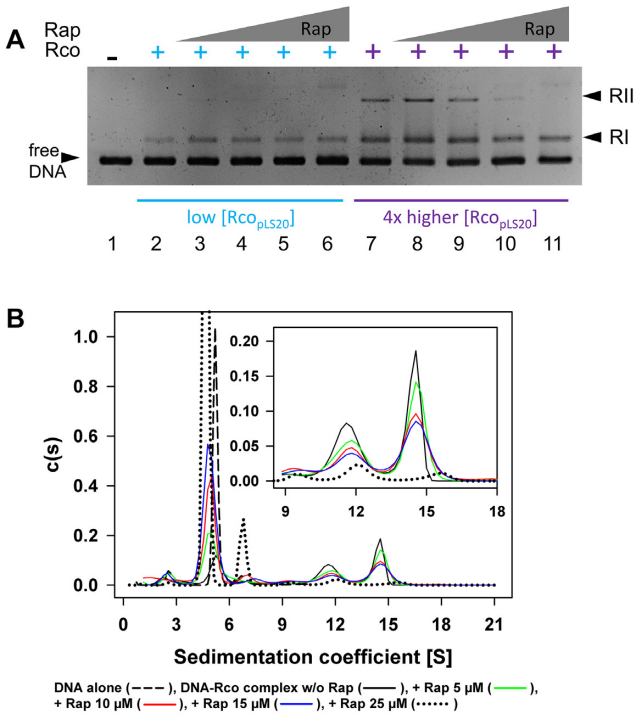

Figure 7. Rap_{pLS20} preferentially disrupts retarded species RII. (**A**) Effect of Rap_{pLS20} on Rco_{pLS20}–DNA and Rco_{pLS20}-sandwiched DNA studied by EMSA. Gel retardations were performed using a DNA fragment encompassing Rco_{pLS20} operator O_{II} (fragment FIII, 219 bp). The DNA fragment was pre-incubated in the absence (–) or presence of either 0.25 μM (blue '+' symbols) or 1 μM (purple '+' symbols) of Rco_{pLS20}. Next, no or increasing concentrations of Rap_{pLS20} was added to the mixtures and, after 10 min incubation, samples were loaded and run on an agarose gel. After running, the gel was stained with EtBr and photographed. Positions of unbound DNA (free DNA), and the retarded species RI and RII are indicated. Increasing concentrations of Rap_{pLS20} were prepared using a two-fold dilution method, and ranged from 0.14 to 1.1 μM. (**B**) Effect of Rap_{pLS20} on Rco_{pLS20}–DNA complexes studied by AUC sedimentation velocity. Sedimentation coefficient distribution at 260 nm, *c*(*s*), corresponding to DNA fragment FIII alone (dashed trace), Rco_{pLS20}–DNA complexes without Rap_{pLS20} (black trace) or with increasing Rap_{pLS20} concentrations: 5 μM (green trace), 10 μM (red trace) and 15 μM (blue trace). Dotted trace stands for sedimentation coefficient distribution at 230 nm, corresponding to an Rco_{pLS20}-DNA pre-incubated mixture with Rap_{pLS20} at 25μM, showing the emergence of free DNA and a Rap_{pLS20}–Rco_{pLS20} complex at 7.1*S*. Inset zooms in the *s*-range encompassing the Rco_{pLS20}–DNA complexes to facilitate comparison of the peak proportions.

DISCUSSION

The family of signal peptide regulated RRNPP proteins contains many members. They all share a similar two-domain structure consisting of a large signal peptide binding C-terminal TPR domain and a smaller N-terminal effector domain. In all RRNPP members studied so far, the direct or indirect transcriptional effects exerted by RRNPP proteins are due to interaction of the N-terminal domain with a target molecule. Binding of the peptide induces allosteric changes in the protein affecting the function of the N-terminal effector molecule (7). Despite these simple basic features, there is an extraordinary plasticity in mechanistic actions, as illustrated by the three RRNPP members that play crucial roles in the regulation of conjugation: PrgX of enterococcal plasmid pCF10, RapI of *B. subtilis* ICEBs1 and Rap_{pLS20} of *B. subtilis* plasmid pLS20 (25–27). The effector domain of PrgX forms a DNA binding helix-turn-helix domain; binding of one of the two competing signal peptides affects DNA binding activity of PrgX, which is

coupled to changes in the oligomerization state of the protein (45,46). RapI activates conjugation of ICE*Bs1* by relieving ImmR-mediated repression of the excision and conjugation genes (25,47). ICE*Bs1* encodes a protease, ImmA, which degrades the ImmR repressor, and overexpression of *rapI* results in excision of a deletion derivative of ICE*Bs1* containing only four genes: *int*, *xis*, *immA* and *immR* (48). However, overexpression of *rapI* did not activate the conjugation genes in the absence of protease-encoding *immA* gene, indicating that RapI stimulates ImmA to degrade ImmR (28). The exact underlying mechanism is unknown. In the case of pLS20, Rap_{pLS20} activates conjugation by relieving Rco_{pLS20}-mediated repression of the conjugation genes (27).

Here we made progress in better understanding the circuitry responsible for regulation of the pLS20 conjugation genes, particularly Rco_{pLS20}-mediated repression of the P_c promoter, and the *in vivo* and *in vitro* role of Rap_{pLS20}. In the first place, we demonstrate that the mode of action of the pLS20-encoded RRNPP protein Rap_{pLS20} acts fundamentally different to those of PrgX and RapI. While PrgX regulates expression of the conjugation genes by binding to DNA, our results show that Rap_{pLS20} does not bind DNA. This excludes the possibility that Rap_{pLS20} might activate the P_c promoter by competing with Rco_{pLS20} for DNA binding. RapI activates conjugative transfer of ICE*Bs1* by stimulating the ICE*Bs1*-encoded protease ImmA to degrade ImmR, the repressor of the conjugation genes. Plasmid pLS20 does not encode a protease required for Rco_{pLS20} degradation, as expression of Rap_{pLS20} was sufficient to relieve Rco_{pLS20}-mediated transcription of the P_c promoter in the minimal *in vivo* regulatory circuitry of the conjugation genes present in strain PKS25 (*amyE*::P_{spank}-rco_{pLS20}, *lacA*::P_{xyl}-rap_{pLS20}, *thrC*::P_c-*lacZ*). The presence and absence of a protease dedicated to degrade the repressor may have intriguing consequences for the conjugation pathway. The ICE*Bs1* encoded ImmR not only represses the conjugation promoter but also activates its own promoter; very low ImmR promoter activity was observed in the absence of ImmR (47). Hence, degradation of ImmR will result in activation of the conjugation genes and simultaneously inhibit *de novo* ImmR synthesis, suggesting that conjugation is an irreversible process. The pLS20 conjugation pathway may be a reversible process or at least it may be more flexible than the ICE*Bs1* system based on the following. Like ImmR, Rco_{pLS20} also represses its conjugation promoter and activates its own expression (34, this work). However, activation of the pLS20 conjugation promoter is not due to degradation of the conjugation repressor but instead is the consequence of sequestration of Rco_{pLS20} by Rap_{pLS20}. Inactivation of Rap_{pLS20} by Phr^*_{pLS20} would result in the release of Rco_{pLS20} from the complex allowing it to bind again to its operators and resuming its transcriptional role. Evidence supporting this has been recently obtained (42). In the second place, we provide evidence that there is cross talk between the conjugation and the competence pathways. Competence is the state in which *B. subtilis* cells are able to bind and stably incorporate extracellular DNA into its genome via homologous recombination (for review see, 49,50). During competence, genes are expressed encoding proteins involved in two functionally separated processes: a membrane-associated DNA translocation machinery that binds exogenous DNA and actively imports ssDNA, and proteins involved in homologous recombination acting on the adsorbed ssDNA. ssDNA is also generated during conjugation and also transported through a membrane-embedded ssDNA translocation machinery, but in the opposite direction to the competence machinery. Various similarities exist between competence and conjugation related ssDNA transfer machines (for review see, 51). However, conjugation and competence development may not be compatible with each other. For example, simultaneous expression and assembly of the competence and conjugation related ssDNA translocation machineries might interfere with each other and/or compete for the same cellular position. In addition, the recombination enzymes synthesized during competence may act on ssDNA of the conjugative element. Importantly, the conjugation operon of pLS20 encodes a protein, Rok_{pLS20} (pLS20cat gene *64*) that represses competence. Thus, activation of the conjugation genes simultaneously inhibits competence development (52). Here, we presented additional evidence showing that conjugation and competence are incompatible processes. In addition to the similarity between Phr^*_{pLS20} and PhrF*, we showed that the mature PhrF* peptide can interact with Rap_{pLS20} *in vitro* provoking Rap_{pLS20} tetramerization as observed for Phr^*_{pLS20} (42), and that the calculated macroscopic K_d of PhrF* is only about 2.5-fold higher than that of Phr^*_{pLS20} (5.3 and 2.1 μM, respectively). Analysis of two synthetic variants of PhrF* containing only one residue difference with Phr^*_{pLS20} revealed that they had a very similar intermediate macroscopic K_d of 4.2 μM, showing that the non-identical residues at positions 2 and 5 contribute in similar proportions to the decreased affinity of PhrF* for Rap_{pLS20}. Importantly, we show that PhrF* was also able to inactivate Rap_{pLS20} *in vivo*, raising the possibility that it may inhibit conjugation under natural conditions. PhrF* is the cognate peptide of chromosomally encoded RRNPP protein RapF, which functions as an inhibitor of the competence pathway by interacting with ComA that stimulates transcription of competence genes (53). Thus, on the one hand PhrF* stimulates competence by inhibiting RapF, and on the other hand we provide evidence here that PhrF* can inhibit conjugation. In summary, competence and conjugation appear to be mutually exclusive processes: activation of the pLS20 conjugation pathway results in the production of Rok_{pLS20} that inhibits competence development, and activation of the competence pathway by PhrF* probably aids in repressing pLS20 conjugation. Interestingly, a σ^H–dependent promoter whose activity increases when cells grown on minimal of sporulation medium enter the stationary phase controls the expression of *phrF* (41,54,55). Here, we have shown that expression of Phr^*_{pLS20} is controlled by two σ^A-dependent promoters P_{rap} and P_{phr} whose activity are highest during exponential growth, and under standard conditions pLS20 conjugation reaches its maximum at the end of the exponential growth phase when cells are growing in rich medium (27).

We have also improved our knowledge regarding transcriptional control of the regulators of the conjugation process. Using transcriptional *lacZ* fusions we have previously shown that P_c is a strong and P_r a weak promoter

(34). Using the more sensitive *gfp* reporter gene, we have now confirmed that P_c and P_r are a strong and weak promoter, respectively. Furthermore, we show that the promoter upstream of rap_{pLS20}, P_{rap}, is a weak promoter and that phr_{pLS20} is under the control of a second promoter, P_{phr}, which is about twice as strong as the P_{rap} promoter. Six out of the seven *B. subtilis* chromosomally located *phr* genes are also known to be controlled by an additional promoter (41). Upon secretion, the Phr peptides diffuse in the surrounding environment. Enhanced production due to the presence of a second *phr*-upstream promoter may be important to compensate for the diffusion-related decrease in concentration. In addition, the signal peptide concentration may be boosted under specific conditions when the *phr* gene is under the control of an alternative σ-dependent factor as is the case for chromosome-encoded *phr* genes (41).

Activation of several differentiation processes including sporulation, competence and motility depend on stochastic variability in expression of a master regulator and is linked to heterogeneity in behavior of genetically identical cells within a culture (56–58). The heterogeneity may lead to so-called bet-hedging strategies resulting in the presence of a subpopulation of differentiated cells even in the absence of conditions favouring the differentiation process, which is beneficial for the community at the population level against possible sudden adverse future conditions. Another evolutionary benefit of heterogeneity is division of labor in which only a subpopulation of cells produces products for the benefit of entire community. However, the process of conjugation is an energy consuming process and has major impacts on cell surface and membrane components, requiring tight repression at times when conditions for successful DNA transfer are not apt. Therefore, heterogeneity-derived mechanisms will not be suitable for controlling conjugation. Indeed, the efficiency of pLS20 transfer is below the detection limit when cells grow under conditions that are antithetical to conjugation (>6 orders of magnitude lower than those observed during optimal conjugation conditions, 27). Notwithstanding, tight repression of the conjugation genes during most of the times should be compatible with rapidly switching on the conjugation process when favourable conditions occur. This is achieved by the combination of multiple-factored regulatory circuit of the conjugation genes. Thus, the strong P_c promoter permits high-level expression of conjugation genes under conjugation favourable conditions. The relatively strong P_{phr} promoter assures the synthesis of rather high levels of the Phr^*_{pLS20} signalling peptide required to compensate for the diffusion effect on concentration, and accurately return conjugation to its default repressed state when conditions for conjugations are no longer apt. The weak P_r and P_{rap} promoters generate low levels of Rco_{pLS20} and Rap_{pLS20}, respectively. This, combined with DNA looping and autoregulatory effects of Rco_{pLS20} on its own synthesis are crucial for proper regulation of the conjugation genes. Low levels of Rco_{pLS20} permit accurate activation of the conjugation genes when appropriate conditions occur. However, low repressor levels will inherently increase fluctuations within and between cells that can affect the tight control. Particularly, DNA looping counteracts this. Due to enhanced local concentration of the regulator, DNA looping simultaneously increases specificity and affinity, and at the same time will control stochasticity of cellular processes (59). Consequently, the particular constellation involving multiple players and levels ensure that the conjugation genes are strictly repressed at most times, but permits accurate activation of the conjugation process when appropriate conditions occur. Using transcriptional *gfp* fusions as reporters to determine promoter activities in individual cells, we show that the P_c promoter became activated rather homogeneously in all or most cells in the population, regardless whether the P_c-*gfp* fusion was placed ectopically on the chromosome, or the *gfp* gene was placed behind the first conjugation gene, gene *28*, on the plasmid. However, several considerations have to be taken into account. First, activation of the P_c promoter does not imply automatically that it will result in conjugative plasmid transfer. For instance, checkpoints may be present downstream the P_c promoter. In addition, even when all conjugation genes are expressed successful transfer may be impeded at several levels, e.g unsuccessful mating pair formation or failure of establishment in the host. Moreover, environmental fluctuations at macro and microscale occurring under natural conditions will affect individual cells or subpopulations that will probably impede population scale activation of the P_c promoter as observed under our laboratory conditions.

Finally, our work furthered our understanding of Rco_{pLS20} DNA binding and looping, and the anti-repressor mechanism of Rap_{pLS20}. We provided compelling evidence that a tetrameric Rco_{pLS20} subunit binds one operator, and that DNA looping occurs due to interactions between two Rco_{pLS20} tetramers bound to both of its operators. Both B2H and AUC results indicated that Rap_{pLS20} and Rco_{pLS20} interact with each other both *in vivo* and *in vitro*. These results are corroborated by our recent SAXS and size exclusion chromatography (SEC) results (42). The AUC SV results and particularly the multi-signal sedimentation velocity (MSSV) demonstrated that the majority of the Rap_{pLS20}/Rco_{pLS20} complexes formed corresponded to one Rap_{pLS20} dimer interacting with one Rco_{pLS20} tetramer. Importantly, AUC and EMSA results demonstrated that Rap_{pLS20} was also able to interact with Rco_{pLS20} when bound to DNA. This interaction did not result in the generation of higher molecular nucleoprotein complexes suggesting that Rap_{pLS20} would alter the mode of Rco_{pLS20} DNA binding. Instead, both the AUC and EMSA approach demonstrated that the addition of Rap_{pLS20} to preformed Rco_{pLS20}-DNA complexes resulted in the release of Rco_{pLS20} from the DNA. In addition, AUC results showed that the release of Rco_{pLS20} from DNA resulted in the concomitant appearance of the Rap_{pLS20}/Rco_{pLS20} complex, demonstrating that Rap_{pLS20} activates the P_c promoter by actively removing Rco_{pLS20} from its operators through the formation of stable heterocomplexes. To fulfil its antirepressive role under natural conditions, Rap_{pLS20} has to act on DNA looping involved Rco_{pLS20} complexes. The EMSA results were interesting in this respect since they indicated that Rap_{pLS20} indeed acted with preference on the Rco_{pLS20} protomers involved in DNA looping.

Rap_{pLS20}-mediated detachment of Rco_{pLS20} from DNA might be achieved and/or accompanied by an alteration in the oligomerization state of Rco_{pLS20}. This is not an

unlikely scenario, because RRNPP-mediated alteration of the oligomerization state has been observed: RapF causes dissociation of ComA dimers, which are the transcriptionally functional form (60–62). However, AUC results showed that molecular weight of the Rap_{pLS20}–Rco_{pLS20} complexes corresponded to a stoichiometry of one Rap_{pLS20} dimer to one Rco_{pLS20} tetramer, strongly arguing that interaction of the Rap_{pLS20} does not affect the oligomerization state of Rco_{pLS20} and hence that Rco_{pLS20} might resume its regulatory role after it is released from the complex in the presence of Phr^*_{pLS20}. This view is indeed supported by our recent SAXS and SEC results showing that the addition of Phr^*_{pLS20} peptide converts the large Rco_{pLS20}–Rap_{pLS20} complex into complexes of smaller sizes that are similar in shape, size and elution volumes of the individual Rco_{pLS20} and Rap_{pLS20} complexes (42). Together these results indicate that Rap_{pLS20} temporarily inactivates the regulatory functions of Rco_{pLS20} through sequestration, and that Phr^*_{pLS20} mediated relief of Rco_{pLS20} allows returning the system to its default conjugation repressed state. This regulation is fundamentally different from the RapI-mediated activation of the ICE*Bs1* element in which RapI does not sequester the repressor but instead causes its degradation by activating the protease ImmA.

SUPPLEMENTARY DATA

Supplementary Data are available at NAR Online.

ACKNOWLEDGEMENTS

We acknowledge the publication fee support of the CSIC Open Access Publication Support Initiative through its '*Unit of Information Resources for Research*' (URICI). We are grateful to Dioniso Ureña for excellent help growing cells overexpressing Rap_{pLS20} and Rco_{pLS20} and helpful advice. We thank Daniel Kearns for providing us with the pMiniMad2 vector, David Rudner for vector pDR110 and pDR111, and Daniel Zeigler of the '*Bacillus Genetic Stock Centre*' (BGSC) for sending us strains and for his advice. Finally, we thank members of the lab for useful discussions.

FUNDING

Ministry of Economy and Competitiveness of the Spanish Government [PID2019_108778GB_C21 (AEI/FEDER, EU) to W.M., PID2019-104544GB-I00 (AEI/FEDER/EU) to C.A.]; Wellcome Investigator grant [209500] to Jeff Errington that supported L.J.W; institutional grants from the 'Fundación Ramón Areces' and 'Banco de Santander' to the Centro de Biología Molecular 'Severo Ochoa'; The funders had no role in study design, data collection and analysis, decision to publish, or preparation of the manuscript. Funding for open access charge: CSIC.
Conflict of interest statement. None declared.

REFERENCES

1. Rutherford,S.T. and Bassler,B.L. (2012) Bacterial quorum sensing: its role in virulence and possibilities for its control. *Cold Spring Harb. Perspect. Med.*, **2**, a012427.
2. Kalamara,M., Spacapan,M., Mandic-Mulec,I. and Stanley-Wall,N.R. (2018) Social behaviours by Bacillus subtilis: quorum sensing, kin discrimination and beyond. *Mol. Microbiol.*, **110**, 863–878.
3. Pottathil,M. and Lazazzera,B.A. (2003) The extracellular Phr peptide-Rap phosphatase signaling circuit of Bacillus subtilis. *Front. Biosci.*, **8**, d32–d45.
4. Grossman,A.D. (1995) Genetic networks controlling the initiation of sporulation and the development of genetic competence in *Bacillus subtilis. Annu. Rev. Genet*, **29**, 477–508.
5. Novick,R.P. and Geisinger,E. (2008) Quorum sensing in staphylococci. *Annu. Rev. Genet.*, **42**, 541–564.
6. Monnet,V., Juillard,V. and Gardan,R. (2016) Peptide conversations in Gram-positive bacteria. *Crit. Rev. Microbiol.*, **42**, 339–351.
7. Neiditch,M.B., Capodagli,G.C., Prehna,G. and Federle,M.J. (2017) Genetic and structural analyses of RRNPP intercellular peptide signaling of Gram-positive bacteria. *Annu. Rev. Genet.*, **51**, 311–333.
8. Dunny,G.M. and Berntsson,R.P. (2016) Enterococcal sex pheromones: evolutionary pathways to complex, two-signal systems. *J. Bacteriol.*, **198**, 1556–1562.
9. Rocha-Estrada,J., Aceves-Diez,A.E., Guarneros,G. and de la Torre,M. (2010) The RNPP family of quorum-sensing proteins in Gram-positive bacteria. *Appl. Microbiol. Biotechnol.*, **87**, 913–923.
10. Declerck,N., Bouillaut,L., Chaix,D., Rugani,N., Slamti,L., Hoh,F., Lereclus,D. and Arold,S.T. (2007) Structure of PlcR: Insights into virulence regulation and evolution of quorum sensing in Gram-positive bacteria. *Proc. Natl. Acad. Sci. U.S.A.*, **104**, 18490–18495.
11. Gallego del Sol,F. and Marina,A. (2013) Structural basis of Rap phosphatase inhibition by Phr peptides. *PLoS Biol.*, **11**, e1001511.
12. Erez,Z., Steinberger-Levy,I., Shamir,M., Doron,S., Stokar-Avihail,A., Peleg,Y., Melamed,S., Leavitt,A., Savidor,A., Albeck,S. *et al.* (2017) Communication between viruses guides lysis-lysogeny decisions. *Nature*, **541**, 488–493.
13. Singh,P.K. and Meijer,W.J. (2014) Diverse regulatory circuits for transfer of conjugative elements. *FEMS Microbiol. Lett*, **358**, 119–128.
14. Johnson,C.M. and Grossman,A.D. (2015) Integrative and conjugative elements (ICEs): what they do and how they work. *Annu. Rev. Genet.*, **49**, 577–601.
15. Lerminiaux,N.A. and Cameron,A.D.S. (2019) Horizontal transfer of antibiotic resistance genes in clinical environments. *Can. J. Microbiol.*, **65**, 34–44.
16. Frost,L.S., Leplae,R., Summers,A.O. and Toussaint,A. (2005) Mobile genetic elements: the agents of open source evolution. *Nat. Rev. Micobiol*, **3**, 722–732.
17. Davies,J. and Davies,D. (2010) Origins and evolution of antibiotic resistance. *Microbiol. Mol. Biol. Rev*, **74**, 417–433.
18. Partridge,S.R., Kwong,S.M., Firth,N. and Jensen,S.O. (2018) Mobile genetic elements associated with antimicrobial resistance. *Clin. Microbiol. Rev.*, **31**, e00088-17.
19. Fernandez-Lopez,C., Bravo,A., Ruiz-Cruz,S., Solano-Collado,V., Garsin,D.A., Lorenzo-Diaz,F. and Espinosa,M. (2014) Mobilizable rolling-circle replicating plasmids from gram-positive bacteria: a low-cost conjugative transfer. *Microbiol. Spectr.*, **2**, 8.
20. Arthur,M., Depardieu,F., Molinas,C., Reynolds,P. and Courvalin,P. (1995) The vanZ gene of Tn1546 from Enterococcus faecium BM4147 confers resistance to teicoplanin. *Gene*, **154**, 87–92.
21. Meijer,W.J.J., Wisman,G.B.A., Terpstra,P., Thorsted,P.B., Thomas,C.M., Holsappel,S., Venema,G. and Bron,S. (1998) Rolling-circle plasmids from *Bacillus subtilis*: complete nucleotide sequences and analyses of genes of pTA1015, pTA1040, pTA1050 and pTA1060, and comparisons with related plasmids from Gram-positive bacteria. *FEMS Microbiol. Rev*, **21**, 337–368.
22. Oskam,L., Venema,G. and Bron,S. (1991) The large *Bacillus* plasmid pTB19 contains two integrated rolling-circle plasmids carrying mobilization functions. *Plasmid*, **26**, 30–39.

23. Koehler,T.M. and Thorne,C.B. (1987) *Bacillus subtilis (natto)* plasmid pLS20 mediates interspecies plasmid transfer. *J. Bacteriol*, **169**, 5271–5278.
24. Dunny,G., Funk,C. and Adsit,J. (1981) Direct stimulation of the transfer of antibiotic resistance by sex pheromones in Streptococcus faecalis. *Plasmid*, **6**, 270–278.
25. Auchtung,J.M., Lee,C.A., Monson,R.E., Lehman,A.P. and Grossman,A.D. (2005) Regulation of a Bacillus subtilis mobile genetic element by intercellular signaling and the global DNA damage response. *Proc. Natl. Acad. Sci. U.S.A.*, **102**, 12554–12559.
26. Shi,K., Brown,C.K., Gu,Z.Y., Kozlowicz,B.K., Dunny,G.M., Ohlendorf,D.H. and Earhart,C.A. (2005) Structure of peptide sex pheromone receptor PrgX and PrgX/pheromone complexes and regulation of conjugation in Enterococcus faecalis. *Proc. Natl. Acad. Sci. U.S.A*, **102**, 18596–18601.
27. Singh,P.K., Ramachandran,G., Ramos-Ruiz,R., Peiro-Pastor,R., Abia,D., Wu,L.J. and Meijer,W.J. (2013) Mobility of the native bacillus subtilis conjugative plasmid pLS20 is regulated by intercellular signaling. *PLos Genet.*, **9**, e1003892.
28. Bose,B., Auchtung,J.M., Lee,C.A. and Grossman,A.D. (2008) A conserved anti-repressor controls horizontal gene transfer by proteolysis. *Mol. Microbiol*, **70**, 570–582.
29. Karimova,G., Ullmann,A. and Ladant,D. (2000) A bacterial two-hybrid system that exploits a cAMP signaling cascade in Escherichia coli. *Methods Enzymol.*, **328**, 59–73.
30. Battesti,A. and Bouveret,E. (2012) The bacterial two-hybrid system based on adenylate cyclase reconstitution in Escherichia coli. *Methods*, **58**, 325–334.
31. Sambrook,J., Fritsch,E.F. and Maniatis,T. (1989) In: *Molecular Cloning: A Laboratory Manual*. Cold Spring Harbor Laboratory Press, NY.
32. Bron,S. (1990) In: Harwood,C.R. and Cutting,S.M. (eds). *Molecular Biological Methods for Bacillus*. John Wiley & Sons Ltd., Chichester, pp. 75–174.
33. Zhang,X.Z. and Zhang,Y.H. (2011) Simple, fast and high-efficiency transformation system for directed evolution of cellulase in Bacillus subtilis. *Microb. Biotechnol*, **4**, 98–105.
34. Ramachandran,G., Singh,P.K., Luque-Ortega,J.R., Yuste,L., Alfonso,C., Rojo,F., Wu,L.J. and Meijer,W.J. (2014) A complex genetic switch involving overlapping divergent promoters and DNA looping regulates expression of conjugation genes of a gram-positive plasmid. *PLoS Genet.*, **10**, e1004733.
35. Schuck,P. (2000) Size-distribution analysis of macromolecules by sedimentation velocity ultracentrifugation and lamm equation modeling. *Biophys. J*, **78**, 1606–1609.
36. Laue,T.M., Shah,B.D., Ridgeway,T.M. and Pelletier,S.L. (1992) In: Harding,S.E., Rowe,A.J. and Horton,J.C. (eds). *Analytical Ultracentrifugation in Biochemistry and Polymer Science*. Royal Society of Chemistry, Cambridge, pp. 90–125.
37. Schuck,P. (2003) On the analysis of protein self-association by sedimentation velocity analytical ultracentrifugation. *Anal. Biochem.*, **320**, 104–124.
38. Balbo,A., Minor,K.H., Velikovsky,C.A., Mariuzza,R.A., Peterson,C.B. and Schuck,P. (2005) Studying multiprotein complexes by multisignal sedimentation velocity analytical ultracentrifugation. *Proc. Natl. Acad. Sci. U.S.A.*, **102**, 81–86.
39. Tataurov,A.V., You,Y. and Owczarzy,R. (2008) Predicting ultraviolet spectrum of single stranded and double stranded deoxyribonucleic acids. *Biophys. Chem.*, **133**, 66–70.
40. Cole,J.L. (2004) Analysis of heterogeneous interactions. *Methods Enzymol.*, **384**, 212–232.
41. McQuade,R.S., Comella,N. and Grossman,A.D. (2001) Control of a family of phosphatase regulatory genes (phr) by the alternate sigma factor sigma-H of Bacillus subtilis. *J. Bacteriol*, **183**, 4905–4909.
42. Crespo,I., Bernardo,N., Miguel-Arribas,A., Singh,P.K., Luque-Ortega,J.R., Alfonso,C., Malfois,M., Meijer,W.J.J. and Boer,D.R. (2020) Inactivation of the dimeric Rap_{pLS20} anti-repressor of the conjugation operon is mediated by peptide-induced tetramerization. *Nucleic Acids Res.*, **48**, 8113–8127.
43. Gago-Cordoba,C., Val-Calvo,J., Miguel-Arribas,A., Serrano,E., Singh,P.K., Abia,D., Wu,L.J. and Meijer,W.J.J. (2019) Surface exclusion revisited: function related to differential expression of the surface exclusion system of bacillus subtilis plasmid pLS20. *Front. Microbiol.*, **10**, 1502.
44. Val-Calvo,J., Luque-Ortega,J.R., Crespo,I., Miguel-Arribas,A., Abia,D., Sanchez-Hevia,D.L., Serrano,E., Gago-Cordoba,C., Ares,S., Alfonso,C. *et al.* (2018) Novel regulatory mechanism of establishment genes of conjugative plasmids. *Nucleic Acids Res.*, **46**, 11910–11926.
45. Kozlowicz,B.K., Shi,K., Gu,Z.Y., Ohlendorf,D.H., Earhart,C.A. and Dunny,G.M. (2006) Molecular basis for control of conjugation by bacterial pheromone and inhibitor peptides. *Mol. Microbiol*, **62**, 958–969.
46. Bae,T. and Dunny,G.M. (2001) Dominant-negative mutants of prgX: evidence for a role for PrgX dimerization in negative regulation of pheromone-inducible conjugation. *Mol. Microbiol.*, **39**, 1307–1320.
47. Auchtung,J.M., Lee,C.A., Garrison,K.L. and Grossman,A.D. (2007) Identification and characterization of the immunity repressor (ImmR) that controls the mobile genetic element ICEBs1 of Bacillus subtilis. *Mol. Microbiol*, **64**, 1515–1528.
48. Lee,C.A., Auchtung,J.M., Monson,R.E. and Grossman,A.D. (2007) Identification and characterization of int (integrase), xis (excisionase) and chromosomal attachment sites of the integrative and conjugative element ICEBs1 of Bacillus subtilis. *Mol. Microbiol.*, **66**, 1356–1369.
49. Dubnau,D. (1991) Genetic competence in *Bacillus subtilis*. *Microbiol. Rev*, **55**, 395–424.
50. Dubnau,D. and Blokesch,M. (2019) Mechanisms of DNA uptake by naturally competent bacteria. *Annu. Rev. Genet.*, **53**, 217–237.
51. Chen,I., Christie,P.J. and Dubnau,D. (2005) The ins and outs of DNA transfer in bacteria. *Science*, **310**, 1456–1460.
52. Singh,P.K., Ramachandran,G., Duran-Alcalde,L., Alonso,C., Wu,L.J. and Meijer,W.J. (2012) Inhibition of Bacillus subtilis natural competence by a native, conjugative plasmid-encoded comK repressor protein. *Environ. Microbiol*, **14**, 2812–2825.
53. Bongiorni,C., Ishikawa,S., Stephenson,S., Ogasawara,N. and Perego,M. (2005) Synergistic regulation of competence development in *Bacillus subtilis* by two Rap-Phr systems. *J. Bacteriol*, **187**, 4353–4361.
54. Carter,H.L.I., Tatti,K.M. and Moran,C.P.J. (1990) Cloning of a promoter used by sigma H RNA polymerase in *Bacillus subtilis*. *Gene*, **96**, 101–105.
55. Cosby,W.M. and Zuber,P. (1997) Regulation of Bacillus subtilis sigmaH (spo0H) and AbrB in response to changes in external pH. *J. Bacteriol.*, **179**, 6778–6787.
56. Korobkova,E., Emonet,T., Vilar,J.M., Shimizu,T.S. and Cluzel,P. (2004) From molecular noise to behavioural variability in a single bacterium. *Nature*, **428**, 574–578.
57. Dubnau,D. and Losick,R. (2006) Bistability in bacteria. *Mol. Microbiol*, **61**, 564–572.
58. Veening,J.W., Smits,W.K. and Kuipers,O.P. (2008) Bistability, epigenetics, and bet-hedging in bacteria. *Annu. Rev. Microbiol*, **62**, 193–210.
59. Vilar,J.M. and Saiz,L. (2005) DNA looping in gene regulation: from the assembly of macromolecular complexes to the control of transcriptional noise. *Curr. Opin. Genet. Dev*, **15**, 136–144.
60. Baker,M.D. and Neiditch,M.B. (2011) Structural basis of response regulator inhibition by a bacterial anti-activator protein. *PLoS. Biol*, **9**, e1001226.
61. Griffith,K.L. and Grossman,A.D. (2008) A degenerate tripartite DNA-binding site required for activation of ComA-dependent quorum response gene expression in Bacillus subtilis. *J. Mol. Biol.*, **381**, 261–275.
62. Wolf,D., Rippa,V., Mobarec,J.C., Sauer,P., Adlung,L., Kolb,P. and Bischofs,I.B. (2016) The quorum-sensing regulator ComA from Bacillus subtilis activates transcription using topologically distinct DNA motifs. *Nucleic Acids Res.*, **44**, 2160–2172.